

Electronic Thesis and Dissertation Repository

9-6-2017 12:00 AM

The *Drosophila melanogaster* model of human uric acid nephrolithiasis as a novel in vivo drug screening platform

Aymon N. Ali, *The University of Western Ontario*

Supervisor: Leong, Hon S., *The University of Western Ontario*

Joint Supervisor: Razvi, Hassan, *The University of Western Ontario*

A thesis submitted in partial fulfillment of the requirements for the Master of Science degree in Surgery

© Aymon N. Ali 2017

Follow this and additional works at: <https://ir.lib.uwo.ca/etd>



Part of the [Translational Medical Research Commons](#)

Recommended Citation

Ali, Aymon N., "The *Drosophila melanogaster* model of human uric acid nephrolithiasis as a novel in vivo drug screening platform" (2017). *Electronic Thesis and Dissertation Repository*. 4905.
<https://ir.lib.uwo.ca/etd/4905>

This Dissertation/Thesis is brought to you for free and open access by Scholarship@Western. It has been accepted for inclusion in Electronic Thesis and Dissertation Repository by an authorized administrator of Scholarship@Western. For more information, please contact wlsadmin@uwo.ca.

Abstract

Nephrolithiasis involves the supersaturation of a stone-forming solute in urine leading to the formation of a calculus. The development of novel therapeutic agents for this multifactorial urological disorder has been hindered by lack of a practical pre-clinical model. Currently established medical treatments can possess unfavorable side effect profiles and inconsistent efficacies in certain metabolic milieus. Here, *Drosophila melanogaster*—an emerging model for calcium oxalate nephrolithiasis—was investigated as a potential disease model and high throughput drug discovery platform for human uric acid nephrolithiasis. Through disruption of the *Uro* gene and purine-rich dietary manipulation, we successfully demonstrate the formation of uric acid calculi in fly malpighian tubules as confirmed by *ex vivo* confocal microscopy, qRT-PCR and scanning electron microscopy. Flies treated with standardized concentrations of drug candidates through a novel assay identified several compounds with potential anti-lithogenic effects underscoring the power of *D. melanogaster* as a high throughput tool in drug screening for nephrolithiasis.

Keywords

Nephrolithiasis, hyperuricemia, *Drosophila melanogaster*, GAL4/UAS system, kidney stone disease, confocal microscopy, insect model, microdissection, drug screening, uric acid, malpighian tubule, urate oxidase

Acknowledgments

I would like to thank the University of Western Ontario and the Department of Surgery for their fantastic MSc in Surgery graduate program. Over the past year, this program has armed me with all the tools necessary to be an excellent academic clinician. It will be a great pleasure to see this unique program grow and evolve in the future.

None of the work I have accomplished would have been possible without the continuous support of my graduate supervisors Dr. Hon Leong and Dr. Hassan Razvi. Hon, thank you for accepting me into the Leong Lab family. Your advice has provided me with true guidance on this long and arduous journey. I could not have done this without you. Dr. Razvi, thank you for your inspiration, mentorship, and having your door open whenever I needed your support. It has been a great experience working with you and the Division of Urology.

I would like to thank the faculty members of the Department of Surgery, especially Dr. Abdel-Rahman Lawandy and Dr. Nicholas Power for their words of encouragement, and Janice Sutherland for always being there to help with my administrative questions.

Lastly, I would like to thank all the members of the Leong Lab for their support, especially Richard Berish, Thamara Dayarathna, Ranjit Padda (assisted with and performed qRT-PCR), Yohan Kim and Janice Gomes. I will always cherish the memory of working with you all.

Abbreviations

AFM	Atomic force microscopy
AFO	Autofluorescent object
BQ	Birefringence quotient
BM	Basement membrane
CCAC	Canadian council on animal care
CKD	Chronic kidney disease
CT	Computerized tomography
CaOx	Calcium oxalate
DM	Drosophila melanogaster
DAPI	4',6-diamidino-2-phenylindole
DMSO	Dimethyl sulfoxide
EGFP	Enhanced green fluorescent protein
EDX	Energy-dispersive X-ray spectroscopy
EG	Ethylene glycol
FTIR	Fourier transform infrared spectroscopy
GAL4	Galactose-responsive transcription factor 4
HGPRT	Hypoxanthine guanine phosphoribosyl transferase
HPLC	High-performance liquid chromatography
HG	Hindgut
MT	Malpighian tubule
MIF	Migration inhibitory factor
MG	Midgut
OC	Optical configurations
PBS	Phosphate-buffered saline
PCR	Polymerase chain reaction
RNA	Ribonucleic acid
SEM	Scanning electron microscopy
TD	Transmitted detector
TS	Tubule segment
UA	Uric acid
UAN	Uric acid nephrolithiasis
UAS	Upstream activation sequence
UAD	Uric acid dihydrate
UTI	Urinary tract infection
URAT1	Urate transporter 1
WT	Wild-type

Table of Contents

Abstract	i
Acknowledgments	ii
Abbreviations.....	iii
Table of Contents	iv
List of Tables	vii
List of Figures	viii
List of Appendices	xi
Chapter 1.....	1
1 Introduction	1
1.1 Classification of nephrolithiasis.....	1
1.2 Physicochemical mechanisms of nephrolithiasis	3
1.3 Uric acid nephrolithiasis	4
1.3.1 Uric acid metabolism.....	5
1.3.2 Risk factors	6
1.3.3 Symptoms and diagnosis	8
1.3.4 Non-surgical management	9
1.4 Current models of uric acid nephrolithiasis	10
1.5 Drosophila melanogaster as a translational model of human disease	11
1.5.1 Comparative functional anatomy of Drosophila melanogaster and human renal systems	13
1.5.2 Role as a model of human nephrolithiasis and renal disease	15
1.5.3 Advantages of D. melanogaster as a model of human renal disease.....	16
1.5.4 Limitations of D. melanogaster based renal modelling.....	18

1.6 Objectives and Hypothesis	20
Chapter 2.....	22
2 Materials and Methods	22
2.1 Rearing and maintenance of <i>D. melanogaster</i>	22
2.2 Preparation of standard and lithogenic fly media	24
2.2.1 Standard media.....	24
2.2.2 Lithogenic media	26
2.3 Gene disruption and knockdown.....	26
2.4 Malpighian tubule dissection and extraction	27
2.5 Quantitative real-time PCR (qRT-PCR)	28
2.6 Determination of the presence of birefringent concretions in fly malpighian tubules and fecal matter	30
2.6.1 Ex vivo imaging of fly malpighian tubules and fecal matter	30
2.7 Stone isolation and scanning electron microscopy/energy dispersive X- ray spectroscopy (SEM/EDX)	32
2.8 Development of high throughput drug screening platform	33
2.8.1 Quantification of birefringence in fly fecal matter	34
2.8.2 Determination of fecal birefringence under varying purine loads ..	36
2.8.3 Determination of effect of DMSO on fecal birefringence	36
2.8.4 Effect of xanthine oxidase inhibitors on malpighian tubule and fecal birefringence.....	37
2.8.5 Drug library screening	37
Chapter 3.....	39
3 Results	39
3.1 Ex vivo imaging of DM malpighian tubules	39
3.1.1 Effect of varying purine loads on birefringent concretion formation	41

3.2	Quantitative real-time PCR	42
3.3	Scanning electron microscopy and energy-dispersive spectroscopy	43
3.4	High throughput drug screening.....	44
3.4.1	Ex vivo imaging of fly fecal matter	44
3.4.2	Effect of DMSO on fecal birefringence	45
3.4.3	Fecal birefringence under varying purine loads	46
3.4.4	Effect of xanthine oxidase inhibitors on formation of birefringent concretions in fly fecal matter and malpighian tubules	47
3.4.5	Drug library screening	48
Chapter 4	50
4	Discussion and conclusions	50
4.1	Ex vivo imaging of DM malpighian tubules	50
4.2	Quantitative real time PCR and Scanning Electron Microscopy/Energy Dispersive X-ray Spectroscopy	52
4.3	Ex vivo imaging of DM fecal matter	53
4.4	Ex vivo imaging of DM malpighian tubules following Allopurinol treatment.....	55
4.5	High throughput drug screening.....	56
4.6	Future directions	57
References or Bibliography	61
Appendices	73
Curriculum Vitae	76

List of Tables

Table 1: Classification of nephrolithiasis by composition, incidence and etiology	3
Table 2 Risk factors and etiologies for uric acid nephrolithiasis (* indicates factor contributing to two or more risk factors).....	8
Table 3 Selected examples of human pathophysiological insights gained from the experimental use of <i>Drosophila melanogaster</i>	13
Table 4 Ingredients used in the preparation of standard media.....	25

List of Figures

Figure 1: Schematic representation of the proposed physicochemical mechanisms of nephrolithiasis.....	4
Figure 2: Purine degradation pathway in human and non-human species	6
Figure 3 Schematic representation of (A) Fly malpighian tubule and tubule segments (B) Principal and stellate cells	14
Figure 4 Functional and structural comparison of: (A) mammalian nephron and (C) insect malpighian tubule; podocyte (B) and nephrocyte (D).	15
Figure 5 The GAL4/UAS system	17
Figure 6 Fly vials maintained in Drosophila incubator at 27° C	23
Figure 7 Malpighian tubule dissection technique	28
Figure 8 Fly fecal matter collection and microscopy	31
Figure 9 Summary of model validation experiments performed	33
Figure 10 Flowchart depicting in silico particle analysis for birefringent area (%) quantification	35
Figure 11 Macro-based automation of birefringence quantification	35
Figure 12 Polarized light micrograph of Uro ^{f04888} and WT flies fed either standard or purine rich medium.....	39

Figure 13 Malpighian tubule crystal formation in under varying dietary conditions.	40
Figure 14 Polarized light micrograph of Uro ^{f04888} fly malpighian tubules following incubation in purine rich medium (1% w/v RNA) showing segmental distribution of birefringent concretions	41
Figure 15 Polarized light micrograph demonstrating Uro ^{f04888} fly malpighian tubule birefringent concretions under varying purine loads	42
Figure 16 Relative Uro gene expression between wild-type Canton S and Uro ^{f04888}	43
Figure 17 Scanning electron microscopy of (A) concretion isolated from Uro ^{f04888} malpighian tubules and (B) Pulverized human uric acid stone with respective EDX spectra.....	44
Figure 19 Fecal birefringence quotient: DMSO vs. controls	46
Figure 20 Fecal birefringence quotient under varying purine loads	46
Figure 21 Fecal birefringence quotient: varying concentrations of allopurinol treated media vs. controls	47
Figure 22 Allopurinol-treated media showing reduced birefringent material in fly malpighian tubules (A) 0.36mM (B) 0.72mM (C) 1.06mM media.....	48

Figure 23 Representative examples: "Yen" algorithm auto-thresholded raw polarized light microscopy images demonstrating fecal birefringence: (A) 2% RNA control (B) Allopurinol (C) test compound "hit".....	49
Figure 24 In vitro grown uric acid dihydrate (UAD) crystals viewed under polarized light microscopy.....	58
Figure 25 In vitro grown L-cystine dihydrochloride crystal admixed with methylene blue under polarized light.....	58
Figure 26 X-ray crystallography of L-cystine based crystal demonstrating characteristic disulfide bond.....	59

List of Appendices

Appendix A1: Permissions, Nature Publishing Group	73
Appendix A2: Permissions, John Wiley and Sons.....	74
Appendix A3: Permissions, Company of Biologists.....	75

Chapter 1

1 Introduction

Nephrolithiasis is a common urological disorder with a lifetime risk of approximately 7-13% in North America, a figure expected to increase to 30% by 2050.¹⁻³ In the United States, the prevalence of stone disease has demonstrated a steady increase from 5.2% (1994) to 8.4% (2012).⁴ Globally, a similar upward trend is observed agnostic of age, sex or ethnic background.⁵ The economic burden of nephrolithiasis is substantial with annual direct costs reported as \$5.3 billion in the United States alone.⁶ Acute nephrolithiasis related complaints generated 1.3 million ER visits in the US (2009), with 20% requiring hospitalization.⁷ In addition to these acute complications, kidney stone disease is also reported to be a source of chronic morbidity associated with chronic kidney disease (CKD).⁸⁻¹⁰ Following the development of an initial kidney stone, the risk of stone recurrence approaches greater than 50% over a period of five years.¹¹

1.1 Classification of nephrolithiasis

Nephrolithiasis is most commonly classified by calculus composition (**Table 1**). Epidemiological data in relation to stone disease is highly variable, reflecting the complex and multifactorial etiologies of this disorder. In industrialized regions, calcium-based calculi are by far the most prevalent, accounting for 80% of all kidney stones.¹²⁻¹⁴ Calcium stones are predominantly composed of calcium oxalate (~70%) in either the monohydrate or dihydrate forms, often in combination with calcium phosphate. Calcium phosphate is the primary constituent of ~10% of

calcium stones.¹⁴ Uric acid (UA) calculi are the second most common, responsible for ~7-10% of kidney stones although significant variations exist geographically, particularly in warmer climates.^{15,16} Struvite calculi, also referred to as “infection-related stones” due to their association with urease-positive organism urinary tract infections (UTIs), comprise ~10% of kidney calculi.¹⁷ The autosomal recessive disorder cystinuria occurs due to defective cystine transport secondary to mutations in the solute carrier genes *SLC3A1* or *SLC7A9* and is responsible for only ~1% of stones^{18,19}. Much rarer stone compositions include silicon, xanthine, protein and drug related stones (triamterene, sulfonamides, indinavir).²⁰

Stone	Potential constituents²⁰	Incidence²	Common etiologies
Calcium oxalate	Monohydrate (Whewellite) Dihydrate (Weddellite)	55-61%	Idiopathic, Low urine volume, Hypercalciuria, Hyperoxaluria, Hypocitraturia ²¹
Calcium phosphate	Brushite PO ₄ /CO ₃ apatite 3/8-calcium phosphate	12-13%	Ca ²⁺ /PO ₄ metabolic disturbances, renal tubular acidosis, UTI ²²
Uric Acid	Uric acid Monosodium urate	8-14%	Low urine pH/volume, Idiopathic, Diabetes,

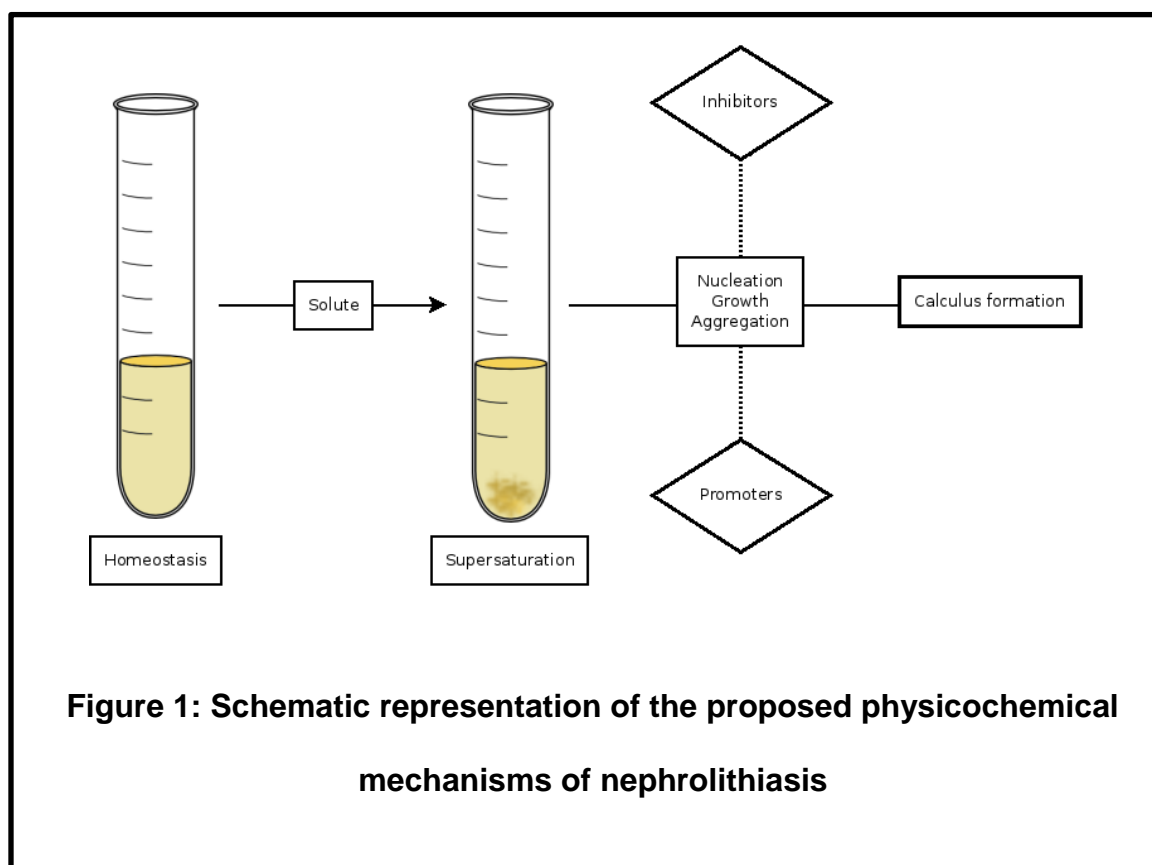
			Hyperuricemia, Dietary, ²³
Struvite	Ammonium- magnesium phosphate	2-6%	Urease-positive UTIs ¹⁷
Cystine	Cystine	1-6%	<i>SLC3A1/SLC7A9</i> mutation ¹⁸
Other	Drugs (e.g. Triamterene), Silicon, Xanthine	<1%	Iatrogenic, Xanthinuria ²⁴

Table 1: Classification of nephrolithiasis by composition, incidence and etiology (North America)

1.2 Physicochemical mechanisms of nephrolithiasis

Despite sizeable nephrolithiasis related costs and morbidity, a complete understanding of nephrolithiasis on the molecular level remains tenuous.^{25,26} Whilst several recent advancements have been made to elucidate the underlying processes involved in stone formation, particularly in relation to calcium and uric acid nephrolithiasis (UAN), the complete cascade of events is yet to be unequivocally defined.²⁷ Several theories exist to describe the journey from solute to calculus, most agreeing with the key starting point of supersaturation of a stone-forming solute in urine promoting crystal formation or crystallization.²⁸ Supersaturation itself is initiated by several etiological factors influencing the

increased production or reduced excretion of the solute in question. This concept, first proposed by Robertson *et al.* in 1966 has persisted as one integral to stone research.^{29–31} This is closely followed by crystal nucleation, growth, and aggregation (**Figure 1**).³² Low-molecular weight compounds such as citrate, stone matrix proteins, pyrophosphate and magnesium can alter the biochemical environment of urine and calculi, modulating stone growth and morphology as a promoter or inhibitor.^{33,34} Urinary pH plays a particularly important role in modifying the solubility of stone forming solutes in urine.³⁵



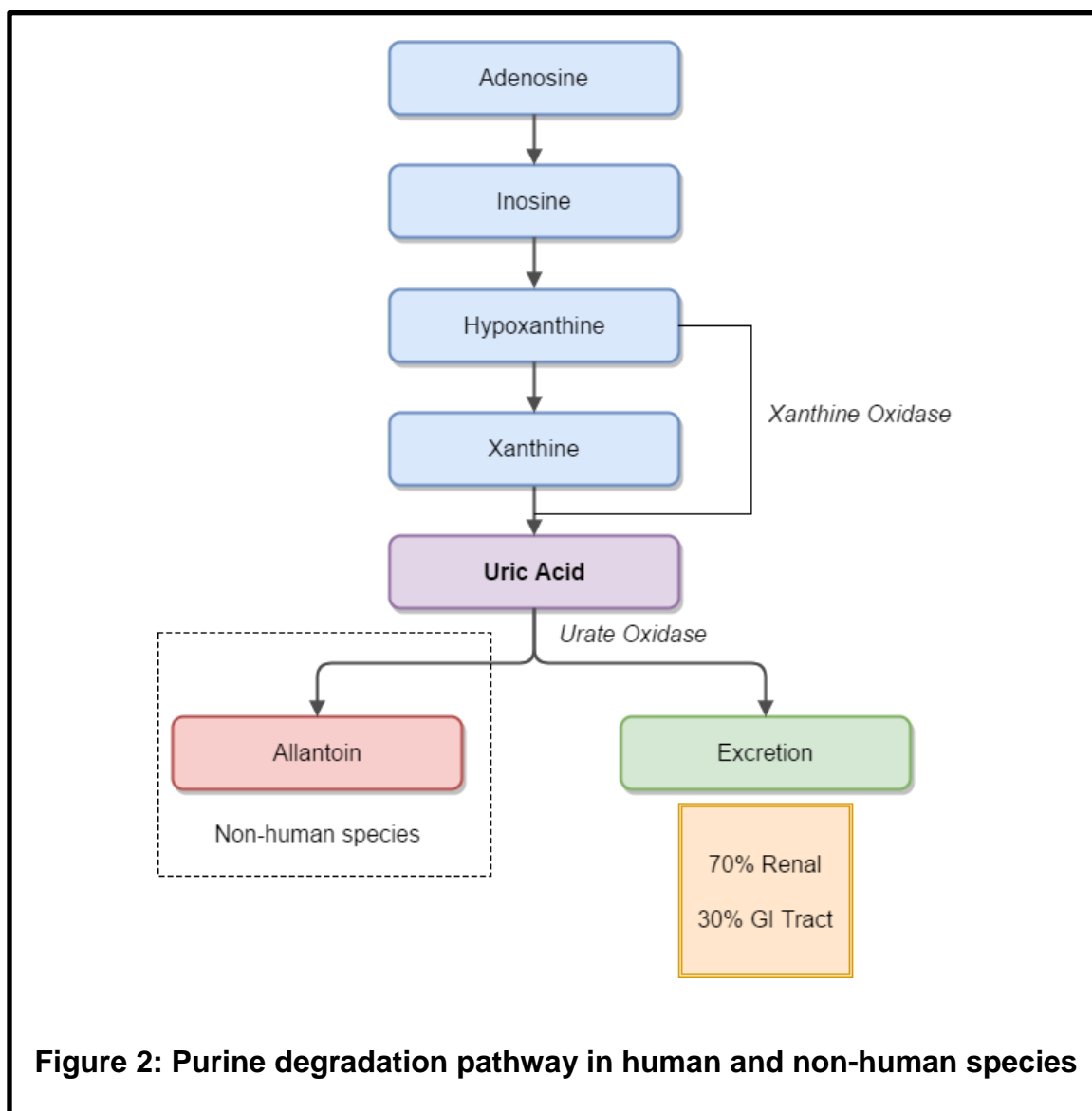
1.3 Uric acid nephrolithiasis

Epidemiological data for uric acid stones varies significantly based on geographical location.³⁶ Regions within the “stone belt” referring to an area spanning from Egypt,

across the Middle East ending at the Philippines appear to be more commonly affected.^{37,38} Prevalence ranges from 4% (Sweden) and 15% (Germany) to as high as 22% and 28.1% in Israel and Pakistan respectively.^{39–42} It is important to note that this data is timeworn (30 years old or more) and new insights into the rapidly evolving epidemiology of uric acid nephrolithiasis are warranted.

1.3.1 Uric acid metabolism

Purines play an important role in human physiology. They are building blocks of the nucleic acids DNA and RNA, are core components of co-enzymes and play a role in neurological and muscular function.⁴³ Uric acid is the end-product of purine metabolism in humans. In lower order mammals and other organisms, uric acid is further metabolized to form the soluble compound allantoin by the enzyme urate oxidase (**Figure 2**).^{44,45} In humans, the gene encoding for urate oxidase production is rendered non-functional due to the presence of two nonsense mutations preventing further metabolism to allantoin.⁴⁶ As a result, humans are hyperuricemic relative to other organisms (10-fold increase).⁴⁷ Uric acid has been shown to possess neuroprotective, anti-oxidant and cardioprotective functions which may explain the evolutionary advantage conferred by the loss of the urate oxidase enzyme and relative hyperuricemia.^{48–51} Following the generation of uric acid, it is freely filtered at the glomerulus and undergoes reabsorption and secretion at the site of the proximal tubule via the URAT1 transporter⁵², ultimately being excreted through the renal and gastrointestinal systems.^{43,53–55}



1.3.2 Risk factors

Several risk factors for uric acid nephrolithiasis have been identified (**Table 2**) however low urinary pH or volume, hyperuricosuria and hyperuricemia are the most strongly associated.^{16,56} With regards to the most important risk factor of low urinary pH^{23,56}, uric acid stone formers have been shown to have a consistently lower urinary pH relative to calcium stone and non-stone formers, despite excreting normal or even lower amounts of uric acid relative to these populations.^{57,58} This phenomenon can be explained by exploring the physicochemical interactions of

uric acid within acidic and basic environments. Uric acid, a weak organic acid (pK_a 5.3 at 37°C), predominantly exists in the ionic form urate within the plasma (physiological pH 7.35-7.45).⁵⁶ Uric acid itself however is poorly soluble in aqueous solutions (~100mg/L) and pH is the single most important determinant of solubility.^{59,60} In contrast, urate is 20 times more soluble.⁶¹ The risk of uric acid crystallization and thus stone formation is therefore inversely related to urinary pH. Hyperuricosuria (24-hour urinary uric acid excretion >600mg/day) can be associated with a wide range of causative factors such as a purine-rich diet (e.g. consumption of large quantities of red meat), hyperuricemia secondary to primary gout and medications.^{16,36,56} Rarer causes include the congenital causes of hyperuricemia such as hypoxanthine guanine phosphoribosyl transferase (HGPRT) deficiency.⁶² Factors contributing to low urine volume such as hypovolemia secondary to sweating and chronic diarrhea increases uric acid supersaturation and thus the risk of uric acid stone formation.^{36,56,63} Neoplastic disorders and other disorders responsible for a high cell turnover have also been identified as potential etiologies.⁶⁴ More recent advancements in the pathophysiology of uric acid nephrolithiasis have identified obesity, type II diabetes and the metabolic syndrome to be associated with an increased risk of stones. This is thought to be due to the association of these disorders with low urinary pH as a result of the renal manifestations of insulin resistance.⁶⁵⁻⁶⁷

Risk Factor	Etiology
Low urine volume	Chronic diarrhea Low fluid intake Diaphoresis
Low urinary pH	Idiopathic Gouty diathesis Diabetes/Metabolic Syndrome Obesity Chronic diarrhea* Primary gout*
Hyperuricosuria	High-purine diet Primary gout* Congenital disorders Medications High cell turnover disorders

Table 2 Risk factors and etiologies for uric acid nephrolithiasis (* indicates factor contributing to two or more risk factors)

1.3.3 Symptoms and diagnosis

The signs and symptoms of uric acid nephrolithiasis are identical to those encountered in nephrolithiasis in general which include acute onset colicky abdominal pain, renal angle tenderness, nausea and hematuria (presence of blood in urine).⁶⁸ As mentioned previously, a low urinary pH (<5.5) may be seen in uric acid nephrolithiasis⁶⁹. Uric acid calculi are radiolucent on plain radiographs⁷⁰, therefore non-contrast helical computerized tomography (CT) scanning is the diagnostic tool of choice⁷¹. Stone analysis can be utilized to confirm the composition of a uric acid based calculus which can be determined by “wet” chemical analysis, FTIR (Fourier Transform Infrared Spectroscopy) and X-ray diffraction.⁷²

1.3.4 Non-surgical management

The non-surgical management of uric acid nephrolithiasis includes urinary alkalinization, lifestyle modification and pharmacological therapy to reduce net uric acid excretion.⁷³ Urinary alkalinization with potassium or sodium citrate/bicarbonate and thus the medical dissolution of uric acid calculi is the first-line treatment in most cases. It is often successful (~70% of cases) and relatively simple to establish.⁷³⁻⁷⁵ For this approach, the urinary pH is maintained between 6.5-7.0, taking care to avoid overalkalinization of the urine as this is associated with an increased risk of developing calcium phosphate calculi. For this reason, carbonic anhydrase inhibitors such as acetazolamide which are also highly capable of urinary alkalinization are generally reserved for patients intolerant to the previously mentioned agents.^{73,76,77} Lifestyle modification in the context of uric acid nephrolithiasis generally refers to nutritional changes such as increasing daily fluid intake and a low purine diet.⁷⁸⁻⁸⁰ Other dietary factors, such as the consumption of sports drinks and grapefruit and other citrus juices could also play a secondary role in the management of uric acid calculi through their alkalinizing and citraturic effects.⁸¹ More recently, theobromine, a methylxanthine found in cocoa and chocolate, has been identified as an inhibitor of uric acid crystallization.⁸² No other urinary inhibitors of uric acid crystallization are currently known apart from some saponins and glycosaminoglycans.⁸² Pharmacological therapy is considered in individuals who continue to develop uric acid calculi despite urinary alkalinization and lifestyle modification.^{73,83} Pharmacological agents primarily include the xanthine oxidase inhibitors allopurinol and febuxostat.⁸⁴ Since the discovery of

febuxostat by the Japanese pharmaceutical company Teijin in 1998, limited advancements have made in the pharmacological management of uric acid nephrolithiasis. Thus, significant efforts have been directed towards the development of novel drug and drug delivery alternatives due to the potential serious adverse effects associated with the use of these agents. These adverse effects include life-threatening hypersensitivity reactions, hepatotoxicity, bone marrow depression and nephrotoxicity.⁸⁵⁻⁸⁷

1.4 Current models of uric acid nephrolithiasis

Several models of hyperuricemia and associated uric acid nephropathy have been described in the literature. The most prominent amongst these are the canine and murine models of UAN. The canine model involves the propensity of a specific breed of dog, the Dalmatian, to ubiquitously excrete high amounts of uric acid in the urine and as a consequence develop uric acid calculi.⁸⁸⁻⁹⁰ This is thought to occur due to a missense mutation in the *SLC2A9* gene, responsible for UA transport at the proximal tubules although other mechanisms such as defective hepatic transport of UA have also been proposed.^{91,92} Whilst there are several advantages to the use of the Dalmatian model such as the similarities between the human and canine genome/pathophysiology, the utility of this model is limited as only ~25% of dogs with hyperuricemia will develop calculi.^{93,94} In addition, higher costs, ethical considerations and the technical difficulties associated with larger mammals apply. A mouse model of hyperuricemia has also been previously described. The mouse model of hyperuricemia involves vector mediated disruption of the urate oxidase gene.⁹⁵ Whilst this process is highly capable of generating

hyperuricemia (10-fold serum uric acid increase), hyperuricosuria and uric acid calculi, undesirable features such as mouse lethality, renal scarring and morphological changes consistent with florid renal failure are also seen. A further rodent model is the rat model of UAN which involves the dietary or intraperitoneal administration of the urate oxidase inhibitor oxonic acid.^{96–98} The administration of oxonate along with dietary uric acid supplementation results in renal calculus formation, hyperuricemia and hyperuricosuria.^{99–104} In addition, renal architectural changes, renal fibrosis, glomerular hypertrophy and cyst formation have been noted.^{98,105} Hyperuricemia can also be induced by adenine and ethambutol administration via gavage.¹⁰⁶ More recently, hyperuricemia has been induced in the tree shrew, a non-rodent mammal of rising research importance, by intraperitoneal oxonic acid administration, however it is unclear whether this approach results in nephrolithiasis.¹⁰⁷

1.5 *Drosophila melanogaster* as a translational model of human disease

Drosophila melanogaster (DM), the common fruit fly, has long been known to be a powerful tool for modeling human disease (**Table 3**). The mapping of the full genome sequence of *Drosophila melanogaster* by Celera Genomics and the *Drosophila* Genome Consortium in March 2000 has resulted in the rapid acceleration of research investigating human disease processes.^{108,109} There is a high degree of genetic conservation between humans and *D. melanogaster*. In fact, 75% percent of human disease-related genes have corresponding items in *D. melanogaster*. Out of 2,309 previously described human disease genes, 700 direct

homologs are present in *D. melanogaster* which also reproduce the human pathology when disrupted.¹¹⁰ In addition, the organ systems of DM, whilst rudimentary, have a remarkable degree of functional and structural similarity to those of humans and retain many of the underlying features.¹¹¹ The application of DM as an investigative tool in this capacity can be seen throughout the literature, especially over the past thirty years.

Field of investigation	Examples
Neurology	Learning and memory ^{112,113} , Frontotemporal dementia ¹¹⁴ , Alzheimer's ¹¹⁵ , Epilepsy ¹¹⁶ , Stroke ¹¹⁷ , Brain tumours ¹¹⁸
Cardiology	Heart development ¹¹⁹ , Congenital heart disease ¹²⁰ , Cardiomyopathy, Heart Failure ¹²¹
Endocrinology	Thyroid cancer ¹²² , Thyroid physiology ¹²³ , Diabetes ¹²⁴
Gastroenterology	Lipid disorders ¹²⁵ , Liver Disease ¹²⁶ , Intestinal dysbiosis/gut microbiome ¹²⁷
Nephrology	Calcium oxalate nephrolithiasis ¹²⁸ , Diabetic nephropathy ¹²⁹ , Kidney injury and repair ¹³⁰ , Xanthinuria ¹³¹

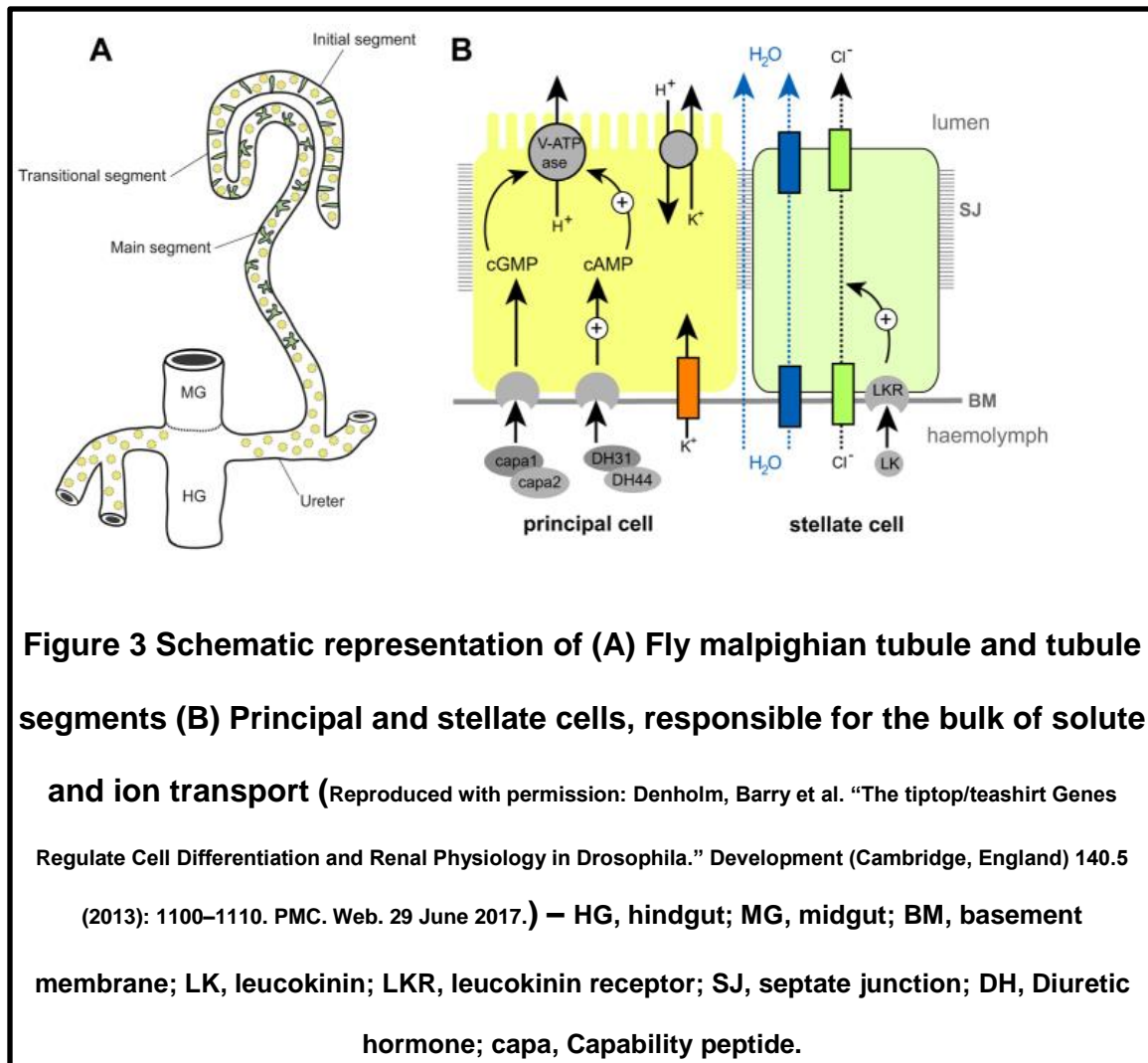
Oncology	Metastasis/metastatic cascade ¹³² , Lung cancer ¹³³
----------	---

Table 3 Selected examples of human pathophysiological insights gained from the experimental use of *Drosophila melanogaster*

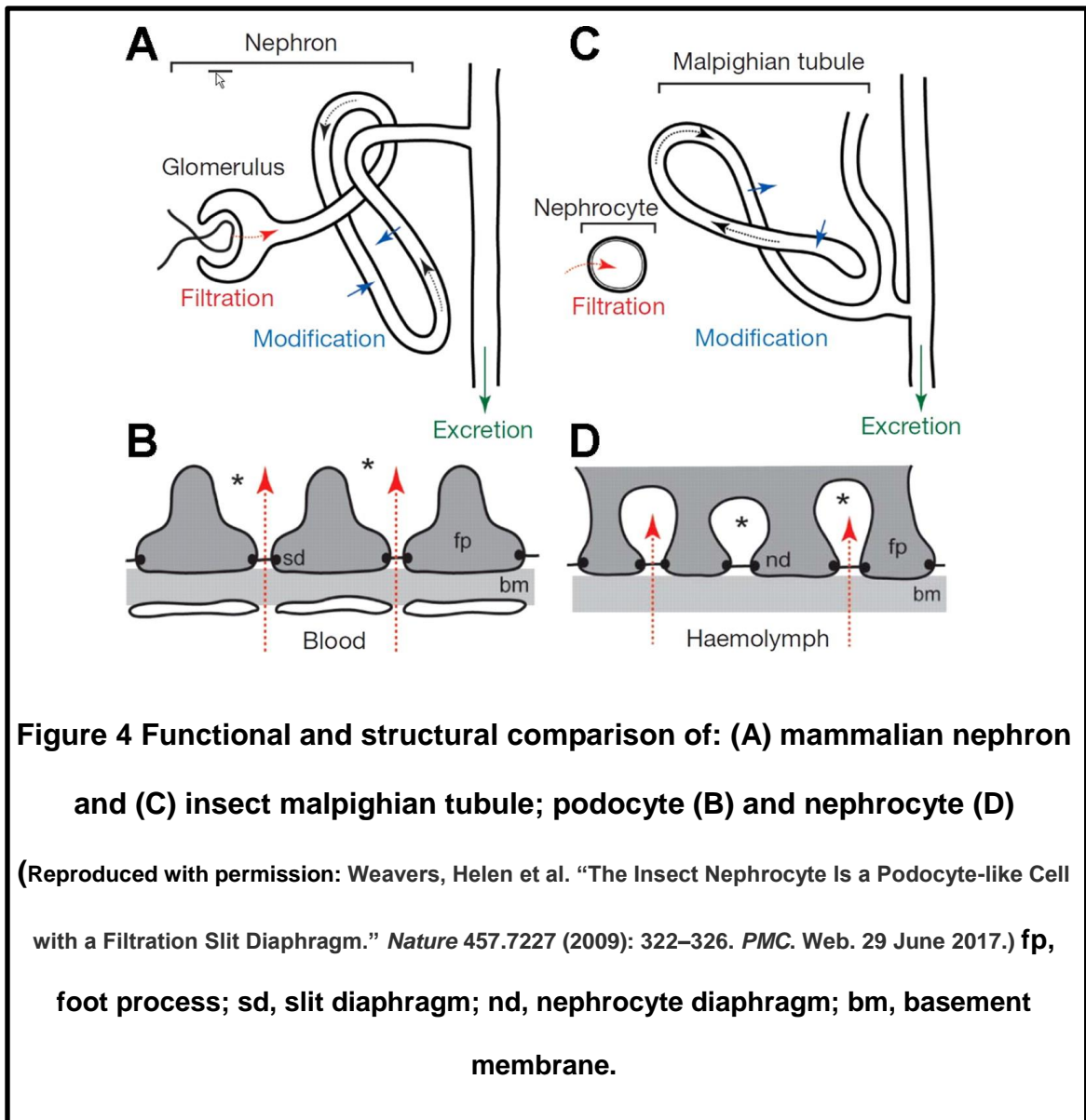
1.5.1 Comparative functional anatomy of *Drosophila melanogaster* and human renal systems

Specialized excretory systems are a fundamental feature encountered in most multicellular organisms. Simplified, these systems aim to maintain biochemical homeostasis by performing the basic functions of filtration, tubular reabsorption and secretion. In *Drosophila melanogaster*, the renal system is composed of two components: Nephrocytes and malpighian tubules (MTs).¹³⁴ Nephrocytes are collections of cells located around the heart (pericardial nephrocytes) and esophagus (garland nephrocytes) that filter fly hemolymph in a manner similar to the human glomerulus.^{131,134,135} Nephrocytes perform this function by virtue of the nephrocyte diaphragm; a filtration structure formed by the nephrocyte plasma membrane invaginations (foot processes) forming small 30nm slit pores in tandem with the nephrocyte basement membrane. Together, the diaphragm and basement membrane form a barrier discriminatory to size and charge analogous to the human glomerulus.¹³⁶ The four malpighian tubules consist of three segments

(initial, transitional and main segments) and two types of cells (principal and stellate cells). **(Figure 3)**



Each pair of MTs further modify the urine via solute and ion transport in a manner similar to the human nephron ultimately excreting waste via a common ureter connected to the fly hindgut.^{130,131,137} **(Figure 4).**



1.5.2 Role as a model of human nephrolithiasis and renal disease

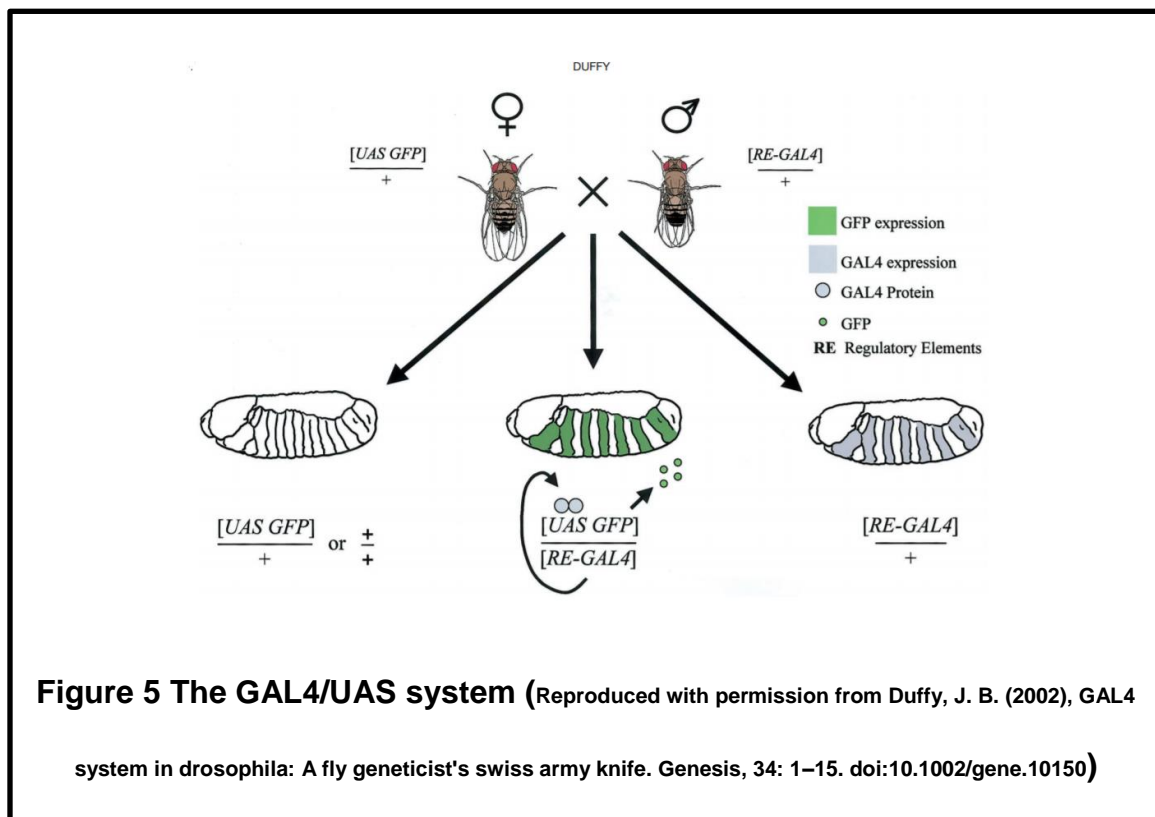
The emergence of *Drosophila melanogaster* as a model for human nephrolithiasis is a relatively recent innovation. The calcium oxalate nephrolithiasis model was first described by Chen *et al.* in 2011.¹²⁸ This model relies on the generation of calcium oxalate (CaOx) crystals in fly malpighian tubules by dietary administration of the lithogenic agents ethylene glycol (EG), hydroxyl-L-proline and sodium oxalate. Birefringent CaOx concretions were visualized *ex vivo* by polarized light

microscopy and chemical composition as CaOx was confirmed by scanning electron microscopy (SEM)/energy-dispersive X-ray spectroscopy (EDX). It was noted that oral administration of potassium citrate ameliorated crystal formation and decreased crystal size. Several further advancements have been made since the initial description of this model. The effect of commercial citrate containing juices was investigated by utilizing the *D. melanogaster* model of calcium oxalate nephrolithiasis and was found to be ineffective in reducing stone burden in comparison to potassium citrate.¹³⁸ In 2015, Chi *et al.* demonstrated that RNAi mediated inhibition of the *Xdh* gene encoding for xanthine dehydrogenase resulted in the formation of concretions in fly malpighian tubules. Through the use of this model, the importance of zinc in the mineralization of stones was discovered.¹³⁹ In addition, the *D. melanogaster* CaOx model has been utilized to identify the role of *dPrestin* (SLC26A6) in luminal oxalate transport by RNAi-mediated silencing of *dPrestin*.¹⁴⁰ *Drosophila* models have also been used to investigate other renal diseases, such as the role of podocyte mutations in the development of the nephrotic syndrome.¹⁴¹

1.5.3 Advantages of *D. melanogaster* as a model of human renal disease

Drosophila melanogaster has occupied a central role in health research over the past century.¹⁴² The genetic tractability of *D. melanogaster* in tandem with the high degree of genetic conservation between fly and human allows for unparalleled investigative ability, manipulation and control through relatively simple techniques.^{143,144} Examples of such techniques include the widely employed

GAL4/UAS system which allows for tissue specific gene regulation e.g. RNAi-mediated gene silencing.^{145,146} This system is composed of two components: the yeast derived *GAL4* gene encoding for the yeast galactose-responsive transcription activating factor protein GAL4 and a responding upstream activation sequence (UAS). A cross between GAL4 and UAS fly results in tissue specific gene regulation.¹⁴⁷ **(Figure 5)**



Other methods include transposon (small, mobile DNA segment)-mediated mutagenesis. Such transposons include *P-elements*, *piggyBacs* and *Minos*, which insert into the genome resulting in disruption/misexpression of adjacent genes.¹⁴⁸ In addition, *Drosophila melanogaster* is amongst the few organisms with a fully mapped genome sequence and several online resources are available which continuously update genetic and genomic knowledge of the *Drosophiladae* family

of flies. The most prominent amongst these groups is the Flybase Consortium which also maintains an active and vibrant community of *Drosophila* researchers.¹⁴⁹ Furthermore, online tools such as Homologene (NCBI), DRSC/DIOPT (Harvard Medical School) and FlyAtlas (Chintapalli, Wang, Dow [University of Glasgow]) are also available to identify tissue specific gene expression and human gene homologs. *Drosophila melanogaster* allows for high throughput study owing to the rapid holometabolous reproductive cycle of DM, which lasts approximately 11 days at 22° C. Rearing and maintenance is inexpensive and requires rudimentary equipment. Fly lines, including transgenic flies, are readily available through major *Drosophila melanogaster* stock centers (Bloomington Stock Center, Indiana, USA., Vienna [Vienna *Drosophila* Research Centre] and National Institute of Genetics, Kyoto, Japan). In relation to the investigation of nephrolithiasis, DM malpighian tubules are transparent and allow for excellent observation of stone disease.¹¹¹

1.5.4 Limitations of *D. melanogaster* renal modelling

The principal apparent limitation of *D. melanogaster* in modelling human renal disease concerns the structural and anatomical arrangement of the renal functional elements in comparison to the human kidney. The *D. melanogaster* renal system has been previously described as an aglomerular system which may have limited the use of DM in this role.^{131,135} The podocyte-like filtration function of *D. melanogaster* nephrocytes has however only recently been described which demonstrates a striking resemblance to the human glomerulus.^{131,134–136} In contrast, unlike the human kidney, these filtration elements (nephrocytes) are not

intimately linked with the modifying tubules (malpighian tubules) and are located at two anatomically distinct sites. This introduces a potential drawback, as a comingling of waste products occurs between the filtered hemolymph and the contents of the fly gut along with modified fluid from the renal tubules prior to their ultimate excretion.¹⁵⁰ This could affect the interpretation of data collected qualitatively or quantitatively from the observation of intact malpighian tubules *in vivo* although methods have been devised to isolate the malpighian tubules *ex vivo* to counter this issue.¹³¹ In addition, the circulatory system of *D. melanogaster* is an open, low-hydrostatic pressure system driven by a single tube-like heart and lacks vascular network.^{151,152} The delivery of fluid to the renal structures is therefore markedly dissimilar to the high-pressure, intravascular system encountered in humans. The complexity of the human diet and associated metabolic processes are difficult to replicate in a rudimentary invertebrate model and as a result, the biochemical milieu encountered in the hemolymph may potentially be markedly different in comparison to human plasma and urine. This limitation is particularly apparent when considering calcium homeostasis in *D. melanogaster* as due to the lack of a skeletal system, approximately one third of the calcium stores of DM are stored within calcium concretions in the anterior malpighian tubules.¹⁵³ Whilst these limitations result in a loss of translational potential and must be considered in any human renal modelling involving *D. melanogaster*, a multitude of human processes are either wholly or partly conserved in *D. melanogaster* and the study of these components could provide novel insights into the human disease equivalent and further management.¹¹⁰

1.6 Objectives and Hypothesis

1) **Generation of uric acid calculi in *D. melanogaster* malpighian tubules:**

We hypothesize that knockdown or disruption of the *Uro* gene encoding for the enzyme urate oxidase via RNAi-mediated silencing or utilization of a mutagenic strain will result in uric acid crystal formation in the malpighian tubules when fed a purine rich diet. This will allow for the observation of uric acid crystals in the malpighian tubules and fly fecal matter due to their negative birefringence under polarized light microscopy.

2) **Confirmation of intervention efficiency:**

We hypothesize that the *Uro* gene expression will be decreased in our knockdown line versus a wild-type fly and will be detectable by qRT-PCR and biochemical methods.

3) **Composition analysis of malpighian tubule concretions versus human uric acid calculi:**

We hypothesize that broad-spectrum protease dissolution of the malpighian tubules will liberate MT crystals, which can be further analyzed by scanning electron microscopy and energy dispersive spectroscopy (EDX) against pulverized human uric acid calculi.

4) **Development of a novel *in vivo* high throughput drug screening assay:**

We hypothesize that a suspended cover slip in fly housing will allow for the collection of fly fecal matter. *In silico* analysis of birefringent area versus

fecal area will allow us to perform a semi-quantitative analysis of stone burden. We hypothesize that treatment with the xanthine oxidase inhibitor allopurinol will reduce stone burden and that the treatment of flies from a nutraceutical drug library of 120 compounds will identify drug candidates for future study.

Chapter 2

2 Materials and Methods

Studies involving the use of the invertebrate *D. melanogaster* are currently exempt from requiring prior approval by an animal ethics board. All animals were handled humanely in accordance with the Canadian Council on Animal Care (CCAC) guidelines (“Guide to the care and use of experimental animals”, 1993).

All fly stocks were sourced from the Bloomington Stock Center, Indiana, USA (<http://fly.bio.indiana.edu>). Canton S flies (Stock #64349) were utilized the wild-type control. Experiments involving the generation of uric calculi utilized the fly line PBac{WH}Uro^{f04888} (Stock #18814) from the Exelixis Collection of transposon insertions. The RNAi fly line UAS-Uro (Stock #67300) along with the GAL4 driver GAL4-Uro (Stock #44416) was used to obtain pilot data. Statistical analysis was performed with GraphPad Prism 6 Software (GraphPad).

2.1 Rearing and maintenance of *D. melanogaster*

All fly stocks were housed in pre-divided trays within wide fly vials (Genesee Scientific Corporation, CA). Stocks were maintained in a temperature controlled environment (27° C) in a dedicated *Drosophila* incubator (DigiTherm® *Drosophila* Incubator, Tritech Research Inc.) (**Figure 6**). A 12-12-hour light-dark cycle and humidity of ~30% was maintained. A supplementary stock of flies was maintained at room temperature. Daily checks were performed to assess for bacterial growth and for the presence of mold or mites in fly housing. Fly media was changed weekly by mass transfer of flies into fresh media. New fly stocks were maintained

in quarantine physically separated from fly lines already in use for at least two generations to prevent mite infestation. Smaller numbers of unwanted flies were disposed of in a fly morgue containing 70% ethanol. For the disposal of larger numbers of flies, flies were culled by freezing at -20°C prior to disposal.



Figure 6 Fly vials maintained in *Drosophila* incubator at 27°C

2.2 Preparation of standard and lithogenic fly media

One-liter volumes of standard fly media were prepared per week. Ingredients were weighed into plastic weigh boats using a digital scale (BL 1500S, Sartorius AG, Germany) and cooked using a laboratory hotplate in a commercial non-stick cooking pot. Following preparation, media was decanted into wide polypropylene vials (GEN32-121, Genesee Scientific, California, USA) using a disposable pipette and covered with grade 50 cheesecloth (GEN53-100, Genesee Scientific, California, USA) whilst cooling. Vials were plugged with cellulose acetate closures (Flugs® GEN49-101, Diamed Inc., Ontario, Canada) and rested at room temperature overnight to prevent water separation. Vials were then stored at 4° C for a maximum duration of 28 days until further use.

2.2.1 Standard media

Standard media was prepared according to the Bloomington #1 formulation described by the Bloomington Stock Center, Indiana, USA (**Table 4**). This formulation results in a firm media which resists liquefaction secondary to larval burrowing.

Ingredient	Quantity
Distilled Water	1000ml (total)
Agar (66-103, Diamed Inc.)	5.76g
Yeast Powder (51475-2.5KG, Sigma Inc.)	17.3g

Soy, powder (62-115, Genesee Scientific)	10g
Cornmeal, yellow (62-100, Genesee Scientific)	73g
Corn syrup, solid (62-109, Genesee Scientific)	76.9g
Propionic acid (1368, Sigma Inc.)	5ml
Tegosept (20-258 Diamed Inc.) 30% solution (optional)	5ml

Table 4 Ingredients used in the preparation of standard media

To prepare standard media, 500ml of distilled water was poured into a non-stick cooking pot and left on high heat to a rolling boil. Cornmeal and agar were combined in a 500ml beaker containing 250ml of distilled water and stirred until a slurry was formed. Yeast and powdered soy were stirred in a separate beaker containing 250ml of distilled water. The cornmeal/agar mixture was added to the boiling water and continuously stirred until a gel-like consistency was achieved. Following this, the yeast/soy mixture was added followed by corn syrup solids. The media mixture was left under high heat until viscous and allowed to cool. Finally, propionic acid was added to the media and mixed thoroughly prior to decanting into fly vials (10ml final volume per vial).

2.2.2 Lithogenic media

For the preparation of lithogenic media, standard media was supplemented with 10g yeast-derived RNA (Sigma-Aldrich, Stock. 10109223001 [Roche]) to yield one liter of 1% w/v RNA media. RNA was added to the media mixture following the addition of the yeast and soy and mixed thoroughly until dissolved. The quantity of RNA added to the media mixture was altered as required to prepare 1%, 2% and 3% w/v RNA media.

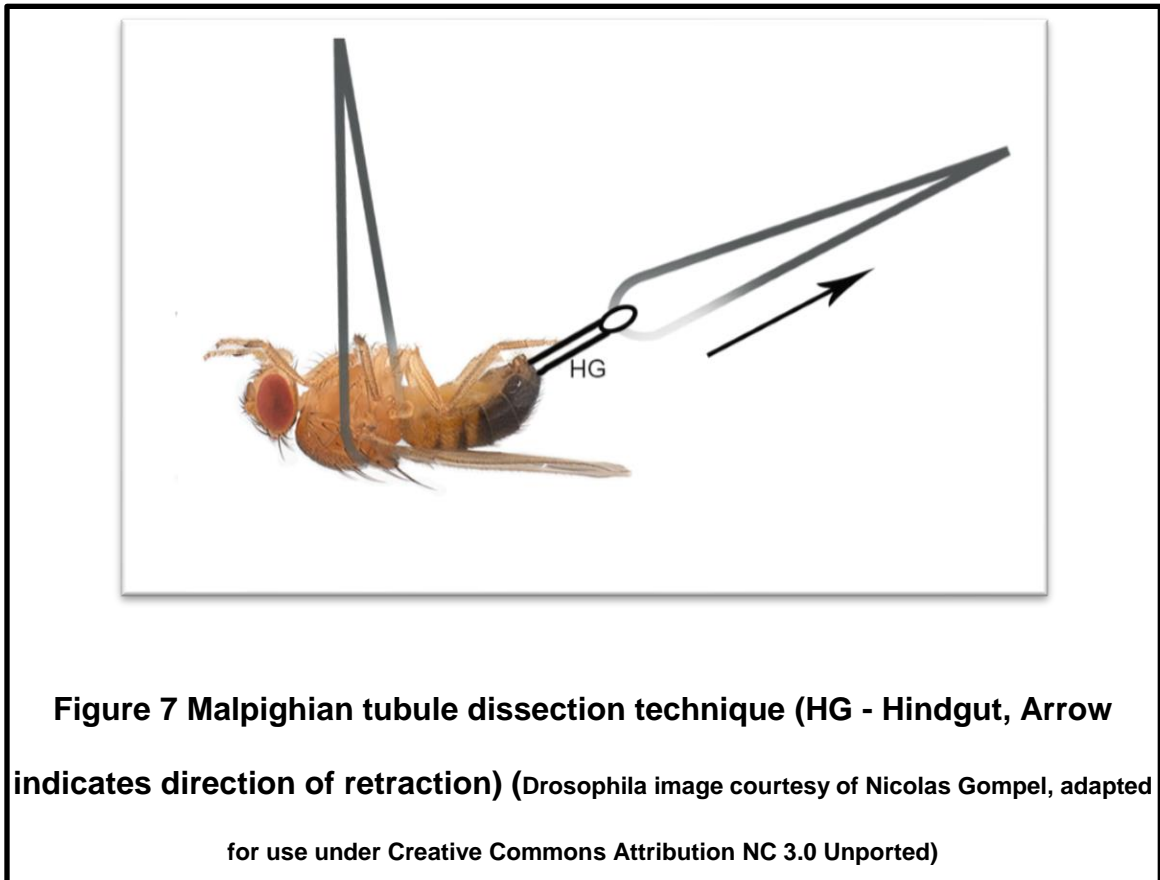
2.3 Gene disruption and knockdown

Disruption of the *Uro* gene was achieved by use of the PBac{WH}Uro^{f04888} fly line from the Exelixis Insertion Collection (Bloomington Stock #18814). This fly line contains an amorphic allele for the *Uro* gene due to the mutagenic activity of the transposon *piggyBac*¹⁵⁴ and was generated in an effort towards developing a complete gene knockdown collection through targeted gene disruption.^{155,156} It has previously been shown that this line possesses a strong loss of function *Uro* mutation.¹⁵⁷ This fly line was utilized for all experiments involving the generation of uric acid calculi unless stated otherwise. Additionally, a GAL4/UAS system RNAi-mediated gene knockdown was investigated by crossing newly eclosed flies from the fly lines UAS-Uro (Stock #63700 – expressing RNAi for Uro under UAS control) and GAL4-Uro (Stock #44416 – donated by J. Dow, expressing GAL4 in the principal cells of the malpighian tubules corresponding to the pattern of urate oxidase). To knockdown the *Uro* gene, vials containing larger numbers of dark pupae were selected from each fly line and flies collected between 8-12 hours after eclosion in a fresh tube containing no media. The flies were then anaesthetized by

CO₂ narcotization (Flystuff Flowbuddy Flow Regulator with Ultimate Flypad, 59-122BCU) and sorted by sex under a dissecting microscope (Amscope Inc., Irvine, United States). Separated flies were added to holding tubes and kept separated for 3 days prior to establishing a cross. The resultant F1 progeny of this cross is expected to have decreased *Uro* expression relative to wild-type flies.

2.4 Malpighian tubule dissection and extraction

Flies were euthanized by CO₂ narcotization (Flystuff Flowbuddy Flow Regulator with Ultimate Flypad, 59-122BCU) and transferred to an empty petri dish in preparation for dissection. Approximately 10ml of phosphate-buffered saline (PBS) was added to an additional Pyrex petri dish (3160100, Sigma-Aldrich Inc.) lined with Sylgard (Dow Corning Inc., Michigan, United States) for dissection. This Petri dish was centered under a dissecting microscope (Amscope Inc., Irvine, United States) with a ringed light source (Amscope Inc., Irvine, United States, LED 144S) to ensure minimal surface glare. Fine Inox steel forceps (Dumont #5, Fine Science Tools Inc., Vancouver, Canada) were utilized to transfer each individual fly to the dissecting petri dish by gently grasping the thorax in a ventral orientation. Using the dominant hand, the anal region was gently grasped and retracted resulting in the emergence of the hindgut followed by the malpighian tubules. **(Figure 7)** The hindgut was severed above the ureters. For experiments requiring the recovery of only the malpighian tubules, the tubules were severed at the ureteric junction. Dissected flies were placed onto a wet sponge. The dissecting forceps were cleaned and dried prior to repeating this process.



2.5 Quantitative real-time PCR (qRT-PCR)

Samples were prepared for qRT-PCR by the dissection and extraction of 30 malpighian tubules from the fly lines *Uro^{f04888}* and wild-type Canton S in triplicate for each group (n=90/group). Six 1.5ml snap top Eppendorf tubes containing 400ul of RNAlater (Sigma Inc., R0901-100ML) were prepared and stored on ice into which malpighian tubules were suspended. If RNA extraction could not be performed the same working day, samples were stored at -80° C and thawed on ice as necessary. PBS was added to each tube in a 1:1 ratio with RNAlater and centrifuged at 15,000 x g for 5 minutes (Eppendorf Minicentrifuge 5548). The supernatant was removed leaving the malpighian tubule pellet at the base of the tube undisturbed. The pellet was disrupted and homogenized using a disposable

micropestle. RNA was extracted by using the RNAeasy Plus Mini Kit (Qiagen, United States) as per the manufacturer's instructions. Total RNA was quantified using a Nanodrop spectrophotometer (ThermoFisher Scientific, United States). One microgram of RNA was reverse transcribed to cDNA with qScript™ cDNA Synthesis Kit (Quanta BioSciences, United States). Real time amplification of 10ng cDNA was performed by the QuantStudio 5 Real-Time PCR system (ThermoFisher Scientific, United States). Each well was loaded with 5µl of SYBR-green master mix (PowerUp SYBR green, Thermo Fisher Scientific), 1µl of each forward and reverse primers (10µM, Thermo Fisher Scientific), 2µl of nuclease free water and 1µl of cDNA. PCR program and conditions consist of 1 cycle of hold stage (50°C for 2 minutes, 95°C for 2 minutes), 40 cycles of PCR stage (denaturation at 95°C for 15 seconds, annealing at 60°C for 1 min) and 1 cycle of melt curve stage (95°C for 15 seconds, 60°C for 1 minute and 95°C for 1 second). Sequence specific primers were used for amplifying the *Uro* gene and are as follows, Forward primer: 5'-GATTCGCAGAAGAACACCGTC-3'; Reverse primer: 5'-TACGCCTCCACATGAACGTG-3'). β -Actin acted as the housekeeping gene (Forward primer: 5'-CTCTGCGGACGCACAATTC-3'; Reverse primer: 5'-TGCAACCAGTCGTCATCTGC-3'). Relative gene expression was calculated from cycle threshold values by $\Delta\Delta$ CT method. Data for relative gene expression *Uro* between *Uro*^{f04888} and wild-type Canton S was collected through the results of three independent experiments.

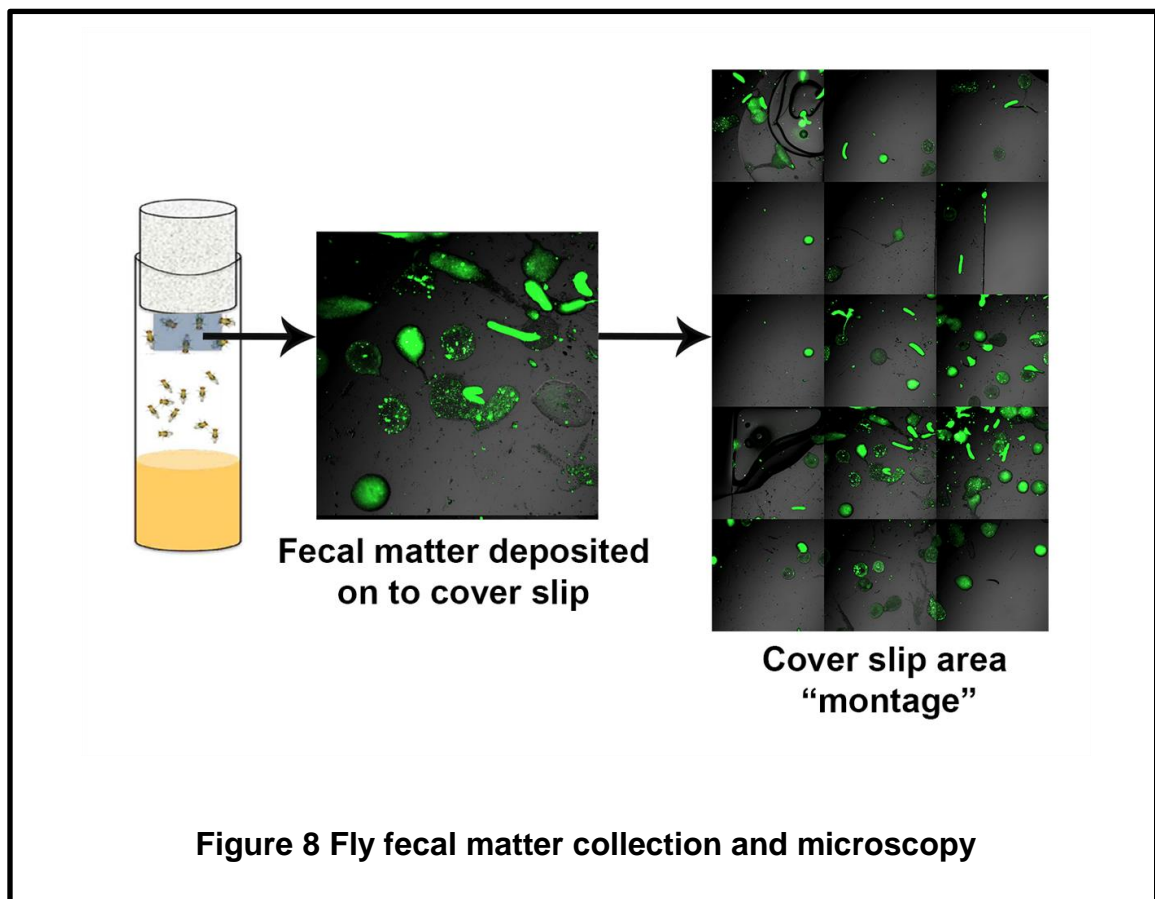
2.6 Determination of the presence of birefringent concretions in fly malpighian tubules and fecal matter

To assess the presence or absence of birefringent concretions in fly malpighian tubules and fecal matter, 20 *Uro*^{f04888} flies were anaesthetized and placed in vials containing 1, 2 and 3% w/v RNA and standard medium in triplicate. Wild-type Canton S was used as a negative control. The cellulose acetate vial closures were scored centrally with a disposable blade to a depth of ~2cm. A clear cover slip was inserted into the scored area and suspended in each fly vial to provide a vertical surface for the collection of fly fecal matter. Each group of flies was allowed to incubate for a period of 10 days after which the malpighian tubules and cover slips were harvested from each group and mounted on to charged glass slides (Superfrost® Plus Microscope Slides, VWR). Each glass slide was prepared for the mounting MTs by pipetting five small droplets (~20ul) of PBS on to the slide to prevent dehydration and degradation of the tubules. Individual droplets were used to mount MTs from a single fly to prevent the MTs from bunching together, improving visualization during microscopy. Tubules were considered crystal positive if birefringence coverage extended over one or more tubule segments to account for any naturally occurring calcium concretions in fly MTs. Suspended cover slips were harvested from each fly vial and dry mounted directly on to glass slides in pairs in preparation for microscopy (**Figure 8**).

2.6.1 *Ex vivo* imaging of fly malpighian tubules and fecal matter

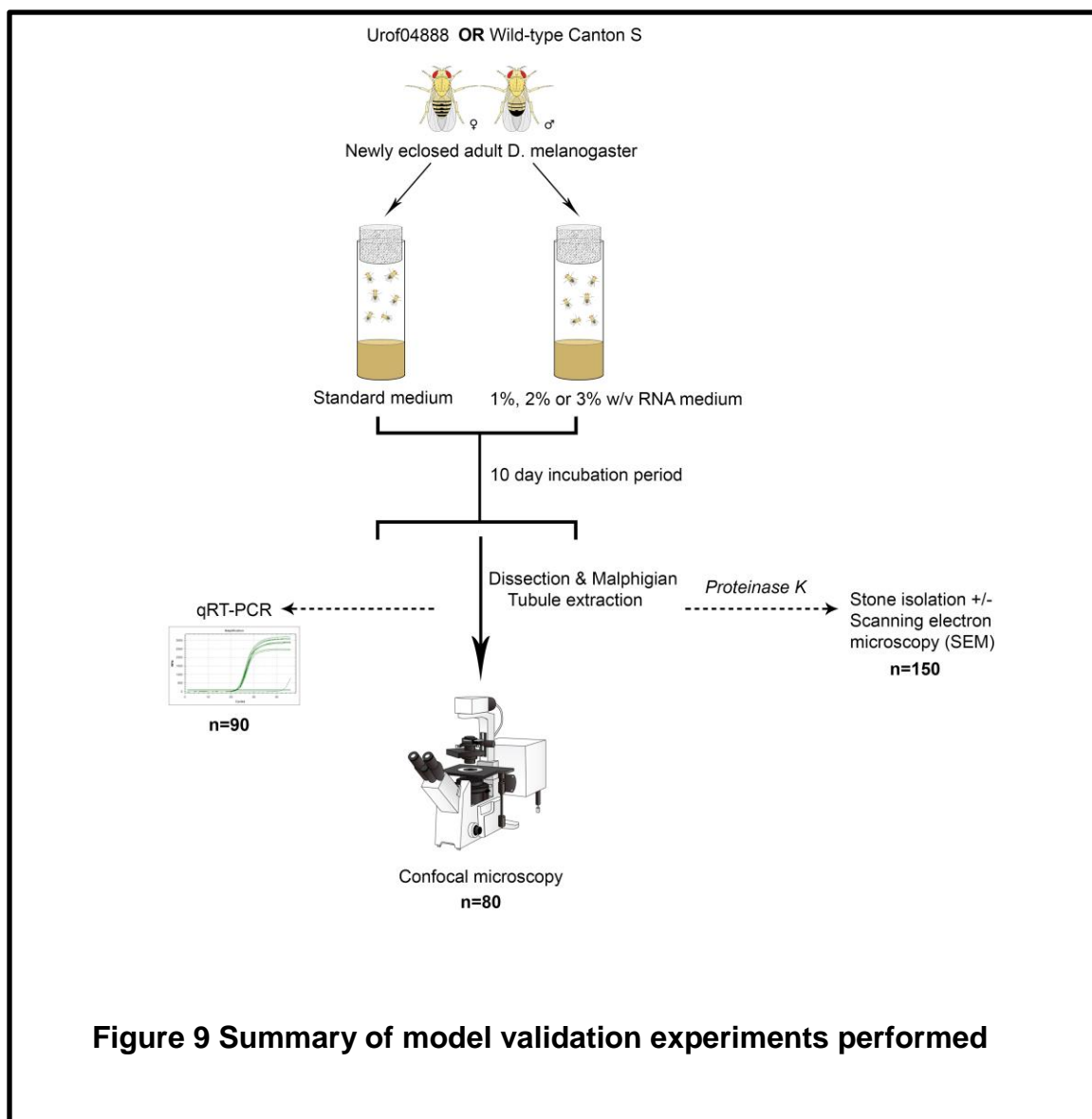
Prepared slides were centered under a confocal microscope (Nikon A1 Confocal Microscope System, Nikon Corp., Japan) at 4X magnification with the transmitted

detector (TD) imaging mode enabled for polarized light microscopy. In addition, fluorescence data was obtained at a single wavelength (EGFP 488nm) to provide contrast. The 4X setting was enabled via the optical configurations (OC panel) and the pinhole was set to 5.3 AU. For the EGFP channel, the gain was set at 105 with an offset -13 and a power of 7.00. For the TD channel, the gain was set at 110 with an offset of -30. The slide was scanned in the resonant mode to bring objects into focus after which the Galvano mode was selected at 2048 pixels and a pixel dwell of 1.2. In the resonant mode, these settings may generate an image which is excessively bright which is corrected in the Galvano mode at the correct pixel dwell. Focus and image plane were finely adjusted using the mouse scroll wheel until the optimal image was obtained.



2.7 Stone isolation and scanning electron microscopy/energy dispersive X-ray spectroscopy (SEM/EDX)

To isolate stones in preparation for scanning electron microscopy (SEM) and analysis of composition, a large quantity of Uro^{f04888} flies (n=150) were dissected following incubation in 1% w/v RNA media for a period of 10 days. The malpighian tubules were suspended in 400ul PBS in a single 1.5ml Eppendorf tube. This sample was centrifuged at 15,000 x g for 5 minutes to form a malpighian tubule pellet at the base of the Eppendorf tube. The supernatant was removed taking care not to disturb the pellet. Following this, 500ul of Proteinase K solution (Proteinase K from *Tritirachium album*, Sigma-Aldrich, P5568-5X1ML) was added to the pellet along with 200ul 0.1% Triton-X solution to dissolve organic tubule material. The pellet was disrupted with a pipette tip and placed capped in a tube hotplate set at 37°C for 24 hours. The sample was re-centrifuged at 15,000 x g for 5 minutes following which the supernatant was removed. The sample was washed with PBS and re-centrifuged two more times to remove any remaining organic material finally being suspended in 500ul UltraPure DNase/RNase free water (Invitrogen). The sample was then submitted for scanning electron microscopy/energy dispersive x-ray spectroscopy along with a pulverized human uric acid stone (confirmed by FTIR) as a positive control at Surface Sciences, Western University, London, Ontario utilizing a Hitachi S4500 Field Emission Scanning Electron Microscope (Hitachi Inc, Tokyo, Japan) and Quartz X One EDX system (Quartz Imaging Corporation).



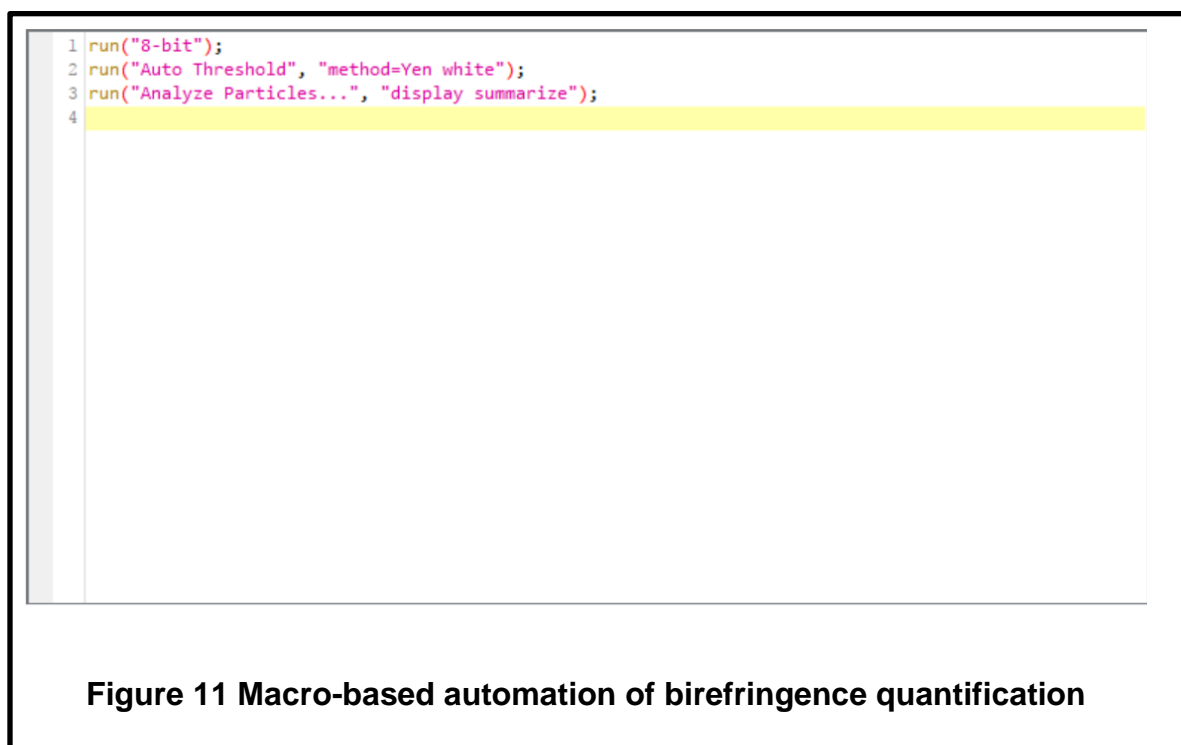
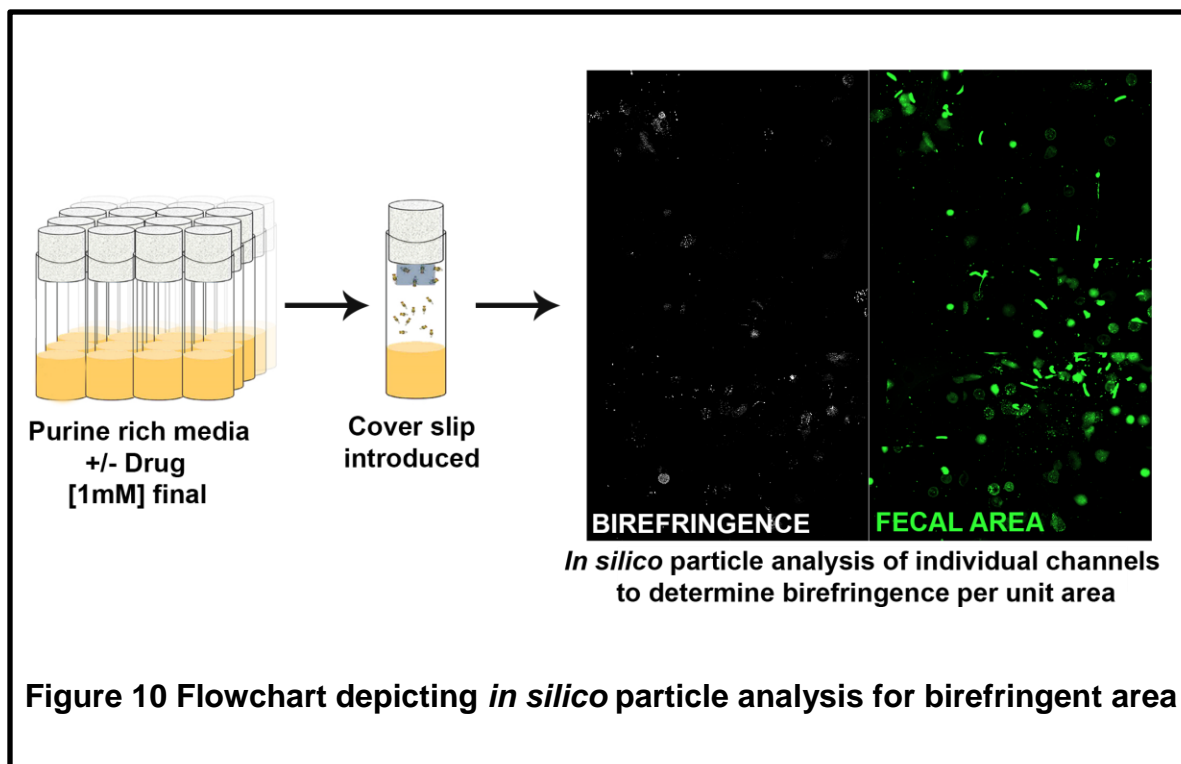
2.8 Development of high throughput drug screening platform

To assess the effect of bioactive compounds on calculus development within the malpighian tubules, a semi-quantitative fecal birefringence assay was developed. As the malpighian tubules ultimately exit into the hindgut via a common ureter, we observed that flies with birefringent concretions in the malpighian tubules also demonstrated birefringent areas in fecal matter. We hypothesized this

birefringence could be used to qualitatively and quantitatively estimate stone burden. To collect fly fecal matter cover slips were suspended from a central score carved into the cellulose acetate closures of fly vials.

2.8.1 Quantification of birefringence in fly fecal matter

To quantify the area of birefringence normalized to total fecal droplet area, an *in silico* image analysis assay was utilized. Initially, the cover slip under investigation was imaged under confocal microscopy. At a 4X magnification, the entire area of the cover slip with fecal matter present could not be imaged in a single visual field. To counter this, the standard process of capturing serial images (~20 images/cover slip) was used followed by software-based stitching in NIS-Elements (File > Stitch Large Image) for further analysis (**Figure 8**). As a motorized stage was not available for use, this process was conducted manually for each cover slip. Each individual image was saved as TIFF file, allowing for the preservation of channel data. Separate montages were generated for the transmitted detector (polarized light) channel and EGFP (488nm wavelength fluorescent data) channels (**Figure 10**). For quantification, ImageJ (NIH – FIJI package) software was utilized by using the particle analysis function, providing numerical output for the area occupied by a particle of interest selected via thresholding. For the transmitted detector channel, a macro was programmed to allow for efficient “single-click” processing (**Figure 11**). This macro automates the processes of changing the image mode to 8-bit grayscale, auto-thresholding via the “Yen” algorithm (eliminating user-bias during thresholding), followed by the “Analyze particles” function, displaying a numerical output.



To analyze the EGFP channel (colored) images, the color thresholding function was used (Image > Adjust > Color Threshold with the "Dark background" option

enabled). The brightness sliders on the thresholding interface were manually adjusted to capture the total fecal area, taking care to exclude very bright green areas representing larvae. This was followed by the executing the “Analyze particles” function. The birefringence quotient (BQ) was calculated by dividing the birefringent area by the total fecal area, providing a value of birefringence per fecal droplet. An empirical qualitative determination of fecal birefringence was also made through direct observation to assess the utility of operator-based judgement to determine relative birefringence.

2.8.2 Determination of fecal birefringence under varying purine loads

To establish controls for future experiments utilizing the fecal birefringence assay, 20 Uro^{f04888} flies were incubated in 1%, 2% and 3% v/w RNA media in triplicate with cover slips suspended from vial closures for the collection of fecal matter for a period of 7 days. Cover slips were collected and imaged as mentioned previously.

2.8.3 Determination of effect of DMSO on fecal birefringence

As future experiments involved the use of dimethyl sulfoxide (DMSO) as a drug solvent, the effect of DMSO on birefringence quotient against a negative control (distilled water) was determined. 1% w/v RNA was prepared and allowed to cool after which 100ul (0.1% v/v) and 200ul (0.2% v/v) of DMSO or distilled water were added and mixed using a pipette tip. These volumes were chosen to match the final volume of drug added during drug screening to ensure any variations in birefringence did not occur as a result of the drug vehicle. 20 Uro^{f04888} flies were

incubated for 7 days in each group of media in duplicate following which the birefringence quotient was determined as previously described.

2.8.4 Effect of xanthine oxidase inhibitors on malpighian tubule and fecal birefringence

The effect of the xanthine oxidase inhibitor allopurinol on the formation of birefringent concretions in fly malpighian tubules and fecal matter was determined by preparing 10ml 2% w/v RNA media as previously described, allowing the media to cool and adding allopurinol (Sigma-Aldrich, A8003-5G) from a stock suspension of 5mM allopurinol after vigorous vortexing to final concentrations of 0.36, 0.72 and 1.06mM. 20 Uro^{f04888} flies were incubated in Allopurinol treated media in duplicate for 7 days after which the malpighian tubules were dissected and cover slips recovered for processing.

2.8.5 Drug library screening

A drug library of 120 nutraceutical compounds was procured through collaboration with Dr. Paul Spagnuolo, Associate Professor, Department of Food Science, University of Guelph. The drug library was received as five 96-well plates loaded with plant-based extracts dissolved in DMSO (24 drugs per plate). Each plate was stored at -80° C until further use. Each drug was labelled via a numbering system to allow for the blinding of prospective researchers, with a master list available upon request. To prepare drug treated media, the entire volume of drug provided (200ul) was added to 5ml 2% RNA media after cooling and homogenized using a pipette tip. Fresh batches of media were prepared for each drug screen and were used immediately after preparation. Twenty-four drugs were tested per week by

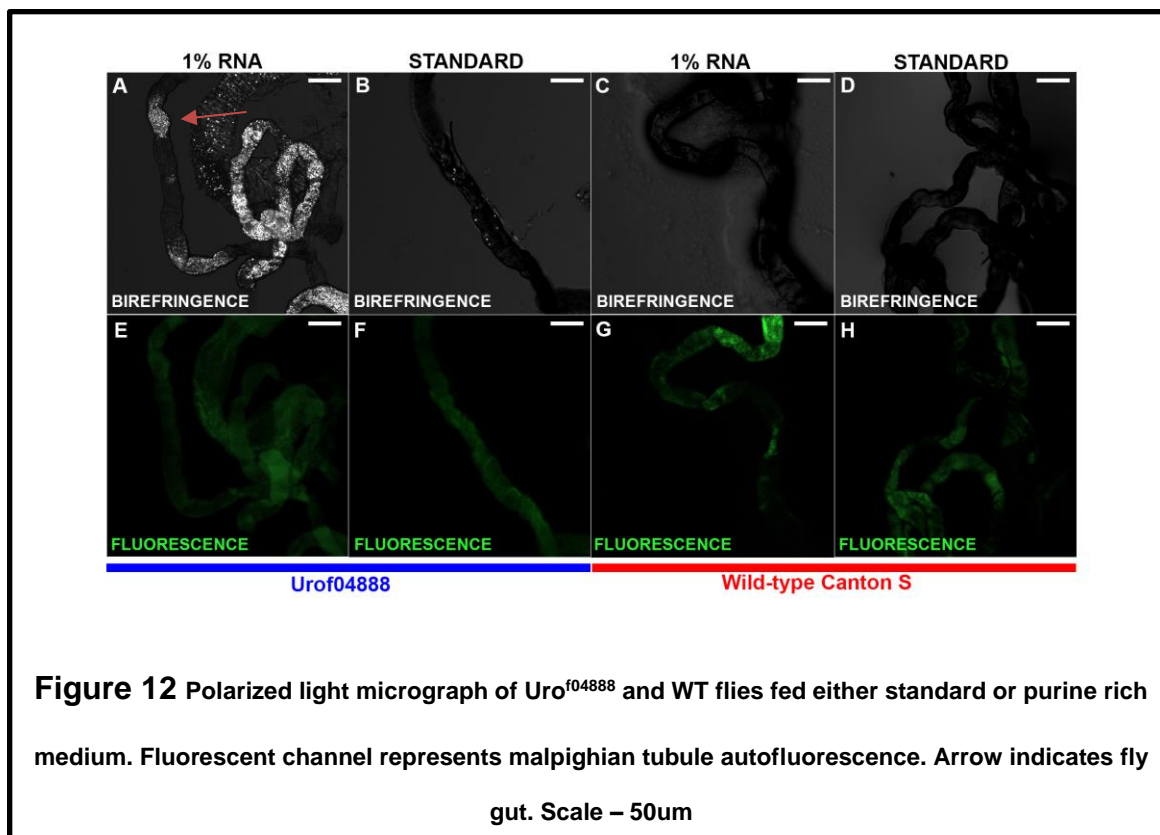
oral administration. This was performed by adding 20 Uro^{f04888} flies to each drug vial, incubating for a period of 7 days. Following this, the birefringence quotient was quantified via the previously described fecal birefringence assay (**Figure 10**). A drug candidate was considered a “hit” if the reduction in birefringence seen was similar in magnitude to that encountered following Allopurinol treatment (little to no birefringent material).

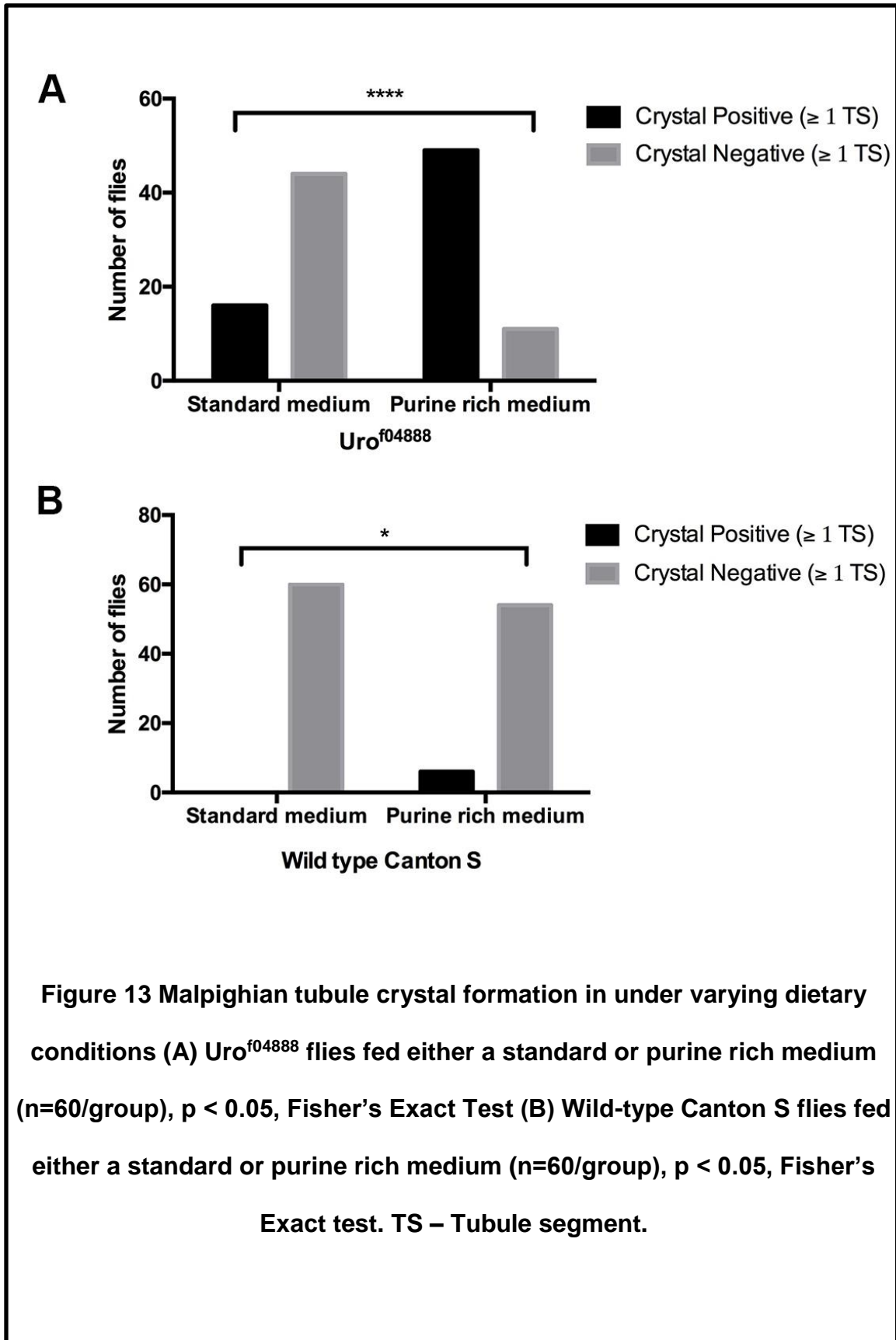
Chapter 3

3 Results

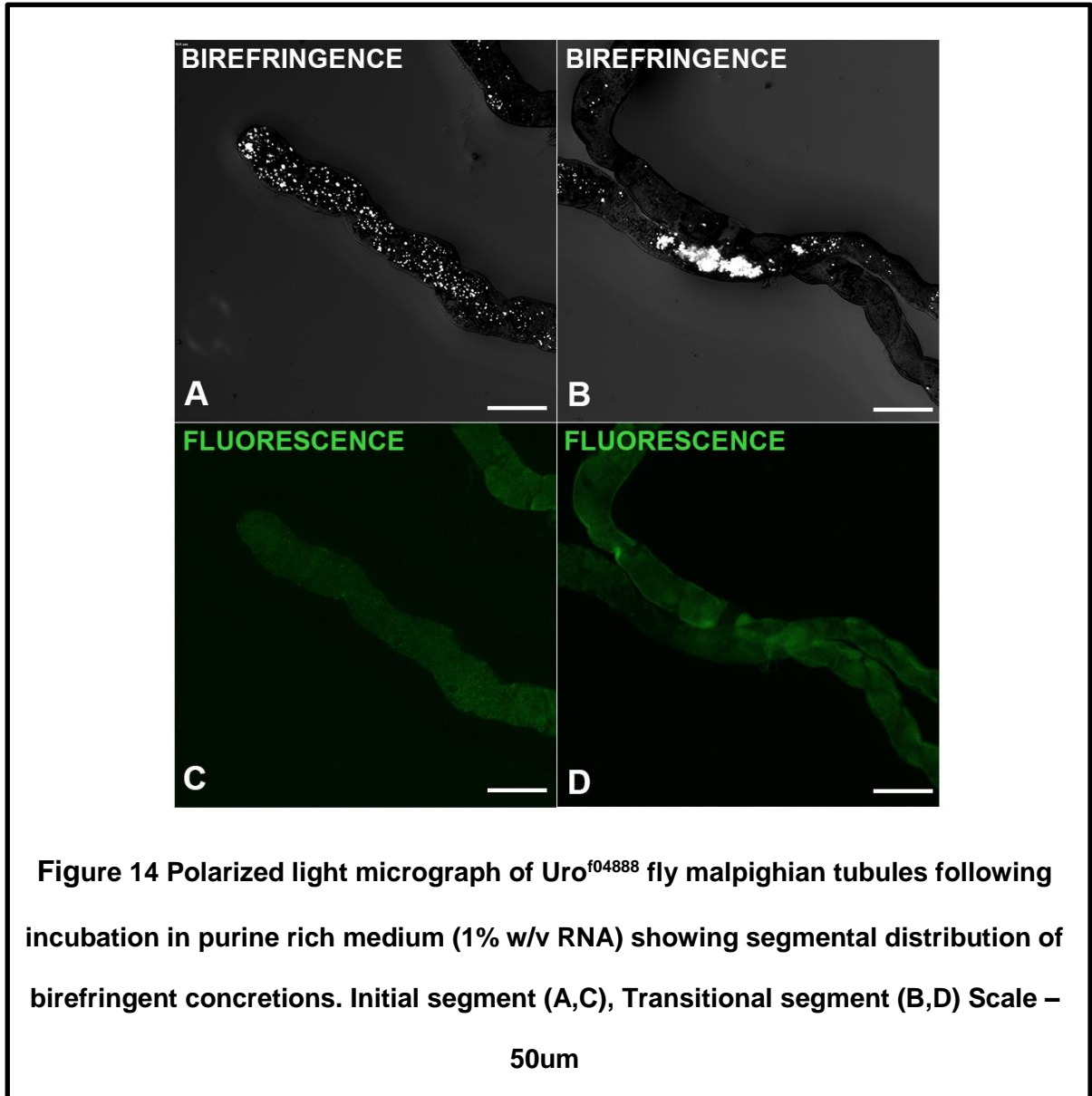
3.1 *Ex vivo* imaging of DM malpighian tubules

Uro^{f04888} flies fed 1% RNA medium demonstrated brilliant birefringence in the malpighian tubules and fly gut (arrow) (**Figure 12 – A, E & Figure 13A**) with crystal coverage extending over one or more tubule segments. In contrast, a paucity of birefringence was noted in *Uro*^{f04888} MTs fed standard medium (**Figure 12 - B, F & Figure 13A**) with a significant difference noted between groups. Smaller to no areas of birefringence were visualized in wild-type (WT) Canton S fly malpighian tubules fed 1% RNA (**Figure 12 - C, G & Figure 13B**). No birefringence was seen in WT fly malpighian tubules when fed standard medium (**Figure 12 - D, H & Figure 13B**).





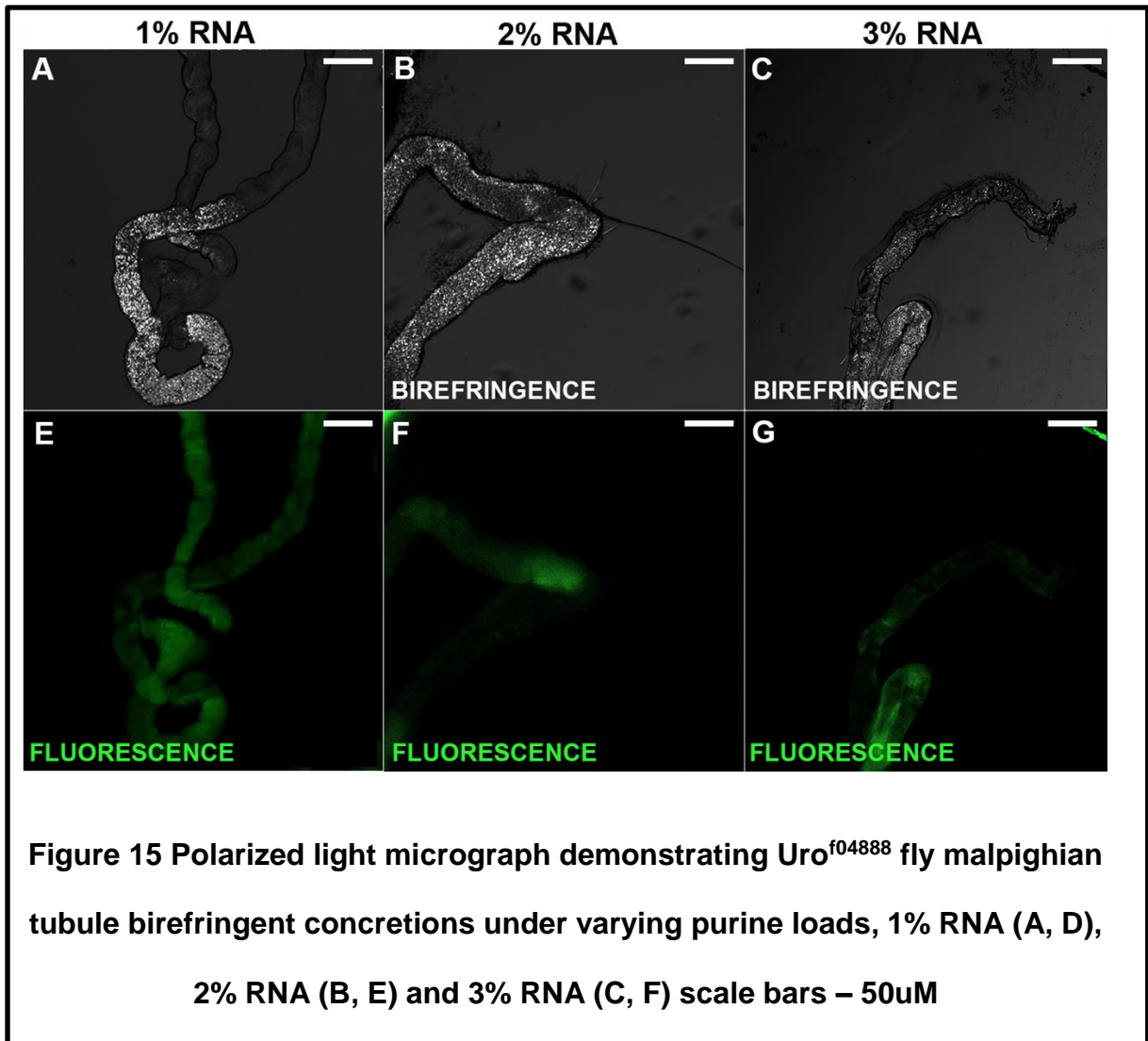
Uro^{f04888} fly tubules showed birefringent concretions in all malpighian tubule segments although the initial (**Figure 14 – A, C**) and transitional (**Figure 14 – B, D**) segments appeared to be particularly affected.



3.1.1 Effect of varying purine loads on birefringent concretion formation

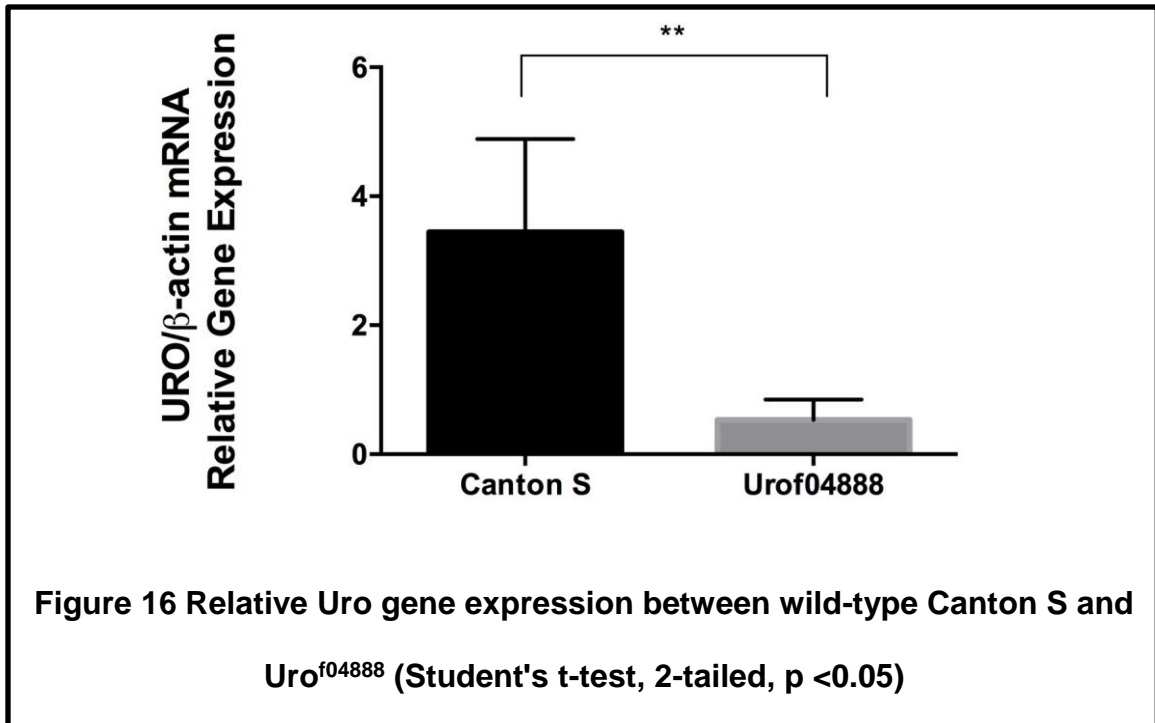
Similar distributions of birefringence were seen across all concentrations of purine rich media (1%, 2% and 3% w/v RNA) in Uro^{f04888} fly tubules (**Figure 15 – A, G**). It

is worth recalling that standard medium, being a yeast-based medium, produced relatively smaller or fewer areas of birefringence extending across one or more tubule segments in *Uro*^{f04888} fly tubules.



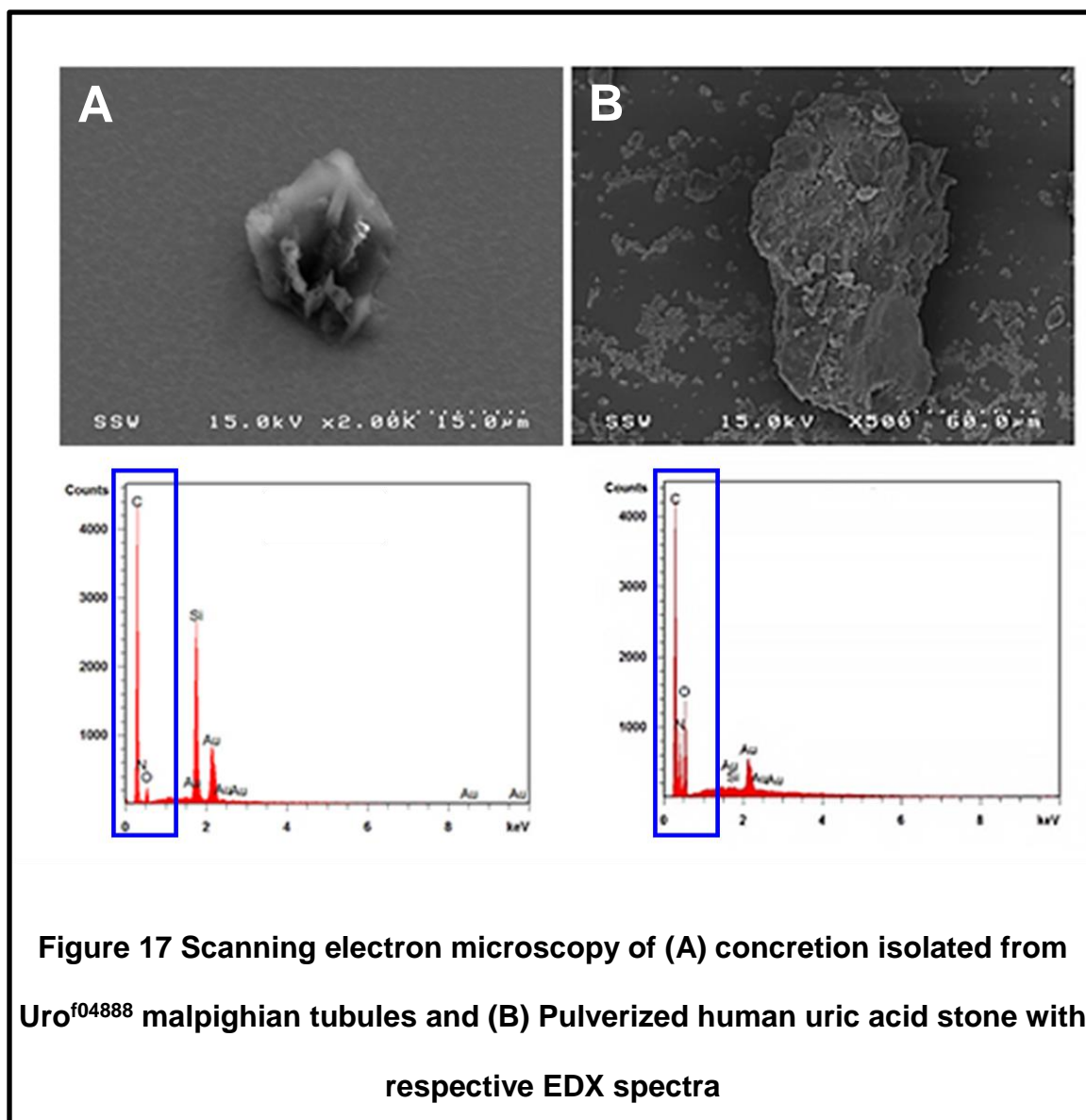
3.2 Quantitative real-time PCR

Quantitative real-time PCR revealed a significant difference in *Uro* gene expression between wild-type Canton S and *Uro*^{f04888} flies (Student's t-test, 2-tailed, $p < 0.05$) with β -actin as the housekeeping gene, accounting for a 74% downregulation of *Uro* gene expression between groups (**Figure 16**).



3.3 Scanning electron microscopy and energy-dispersive spectroscopy

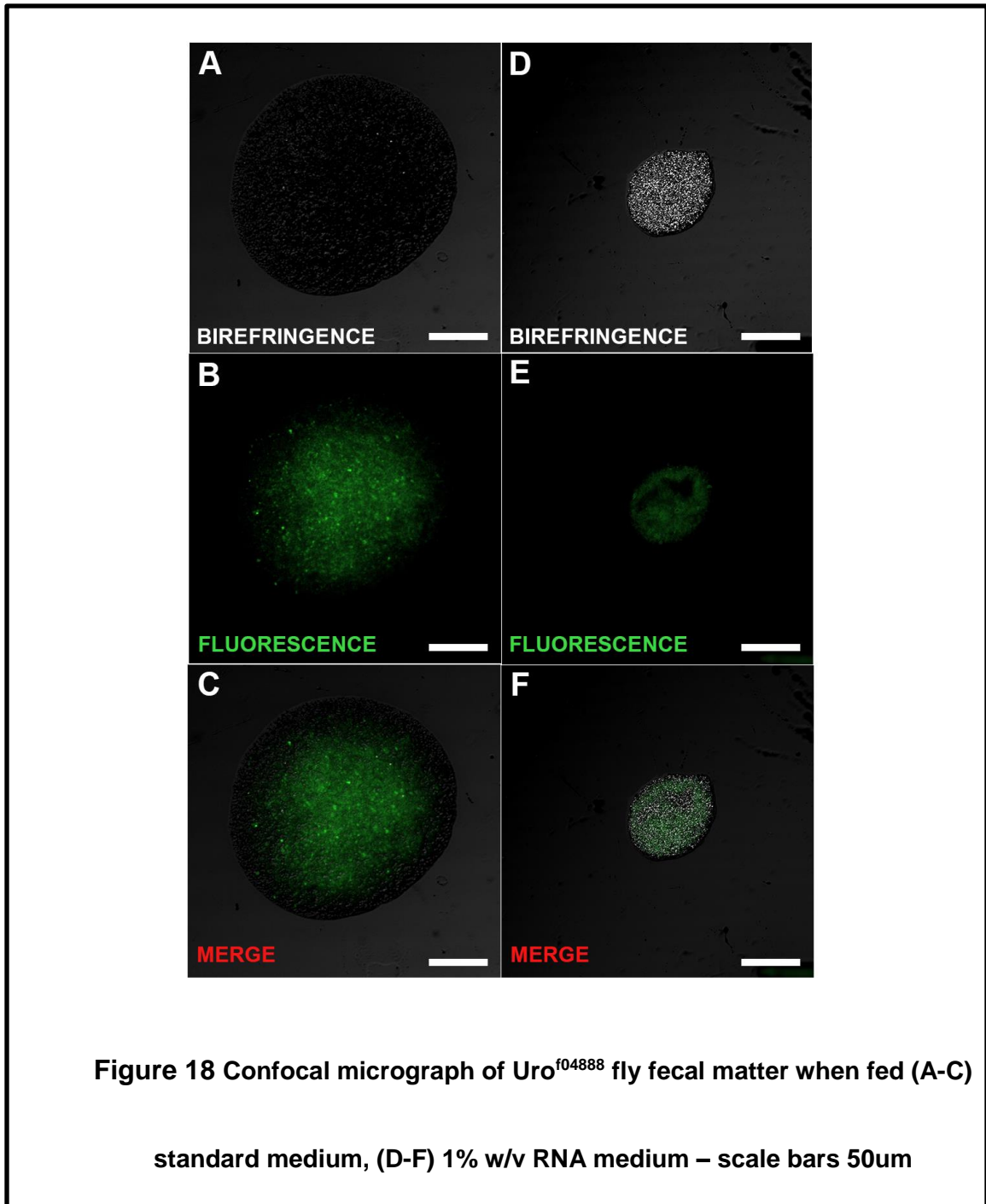
Birefringent concretions were isolated from Uro^{f04888} fly malpighian tubules as previously described and subjected to scanning electron microscopy and energy dispersive spectroscopy (**Figure 17, A**). A pulverized human stone sample previously confirmed as being predominantly composed of uric acid by Fourier transform infrared spectroscopy (FTIR) was used as a positive control (**Figure 17 - B**). Scanning electron microscopy and energy dispersive X-ray spectroscopy of isolated MT concretions against a pulverized human uric acid calculus both demonstrated similar elemental compositions consisting of carbon (C), nitrogen (N) and oxygen (O), consistent with uric acid. Silicon (Si) and Gold (Au) peaks seen are a result of noise generated through the mounting process for scanning electron microscopy.



3.4 High throughput drug screening

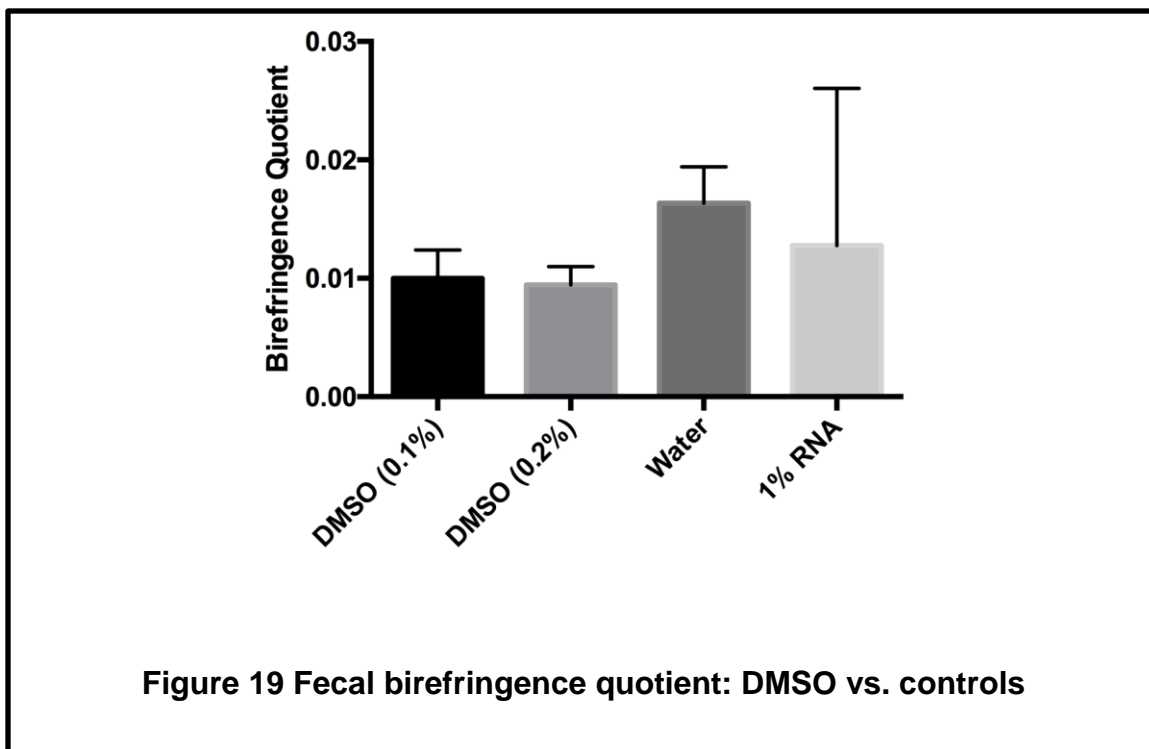
3.4.1 *Ex vivo* imaging of fly fecal matter

Fly fecal matter collected from *Uro^{f04888}* flies fed 1% w/v RNA media for a period of 7 days demonstrated diffuse brilliant birefringence throughout the entirety of the fecal volume (**Figure 18, D-E**). In flies fed standard medium, small foci of birefringence were seen, correlating with findings encountered during malpighian tubule dissection. (**Figure 18, A-C**).



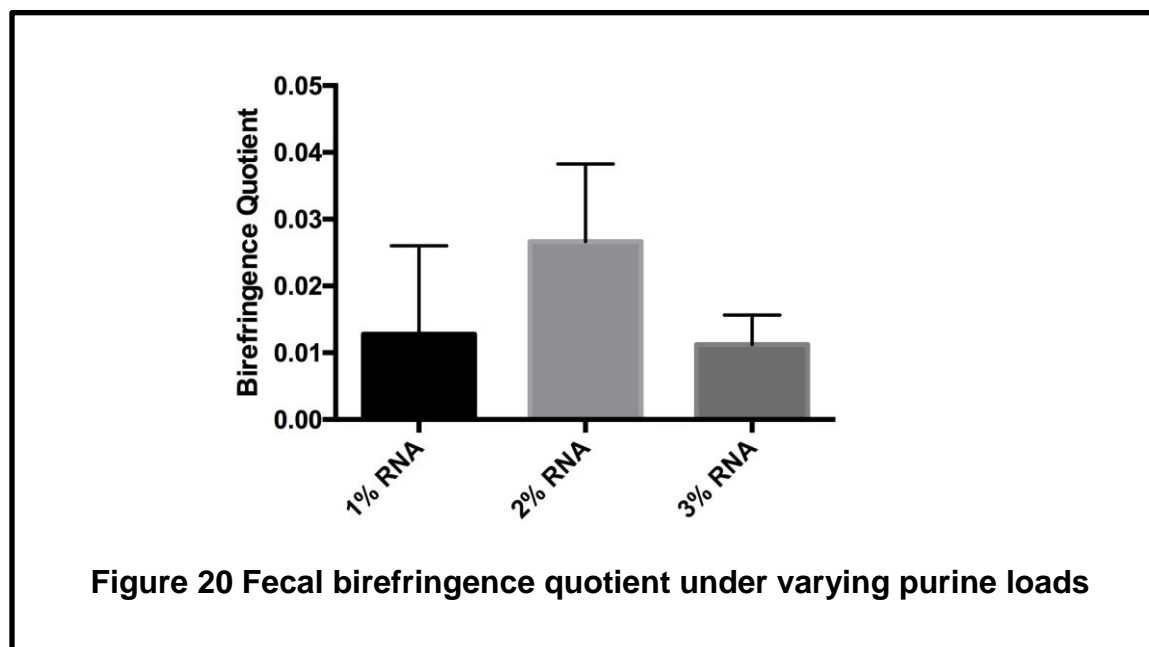
3.4.2 Effect of DMSO on fecal birefringence

No significant difference in fecal birefringence quotient was seen between 0.1% and 0.2% v/v DMSO media groups vs. controls (One-way ANOVA, Tukey's multiple comparisons, $p > 0.05$.) (**Figure 19**).



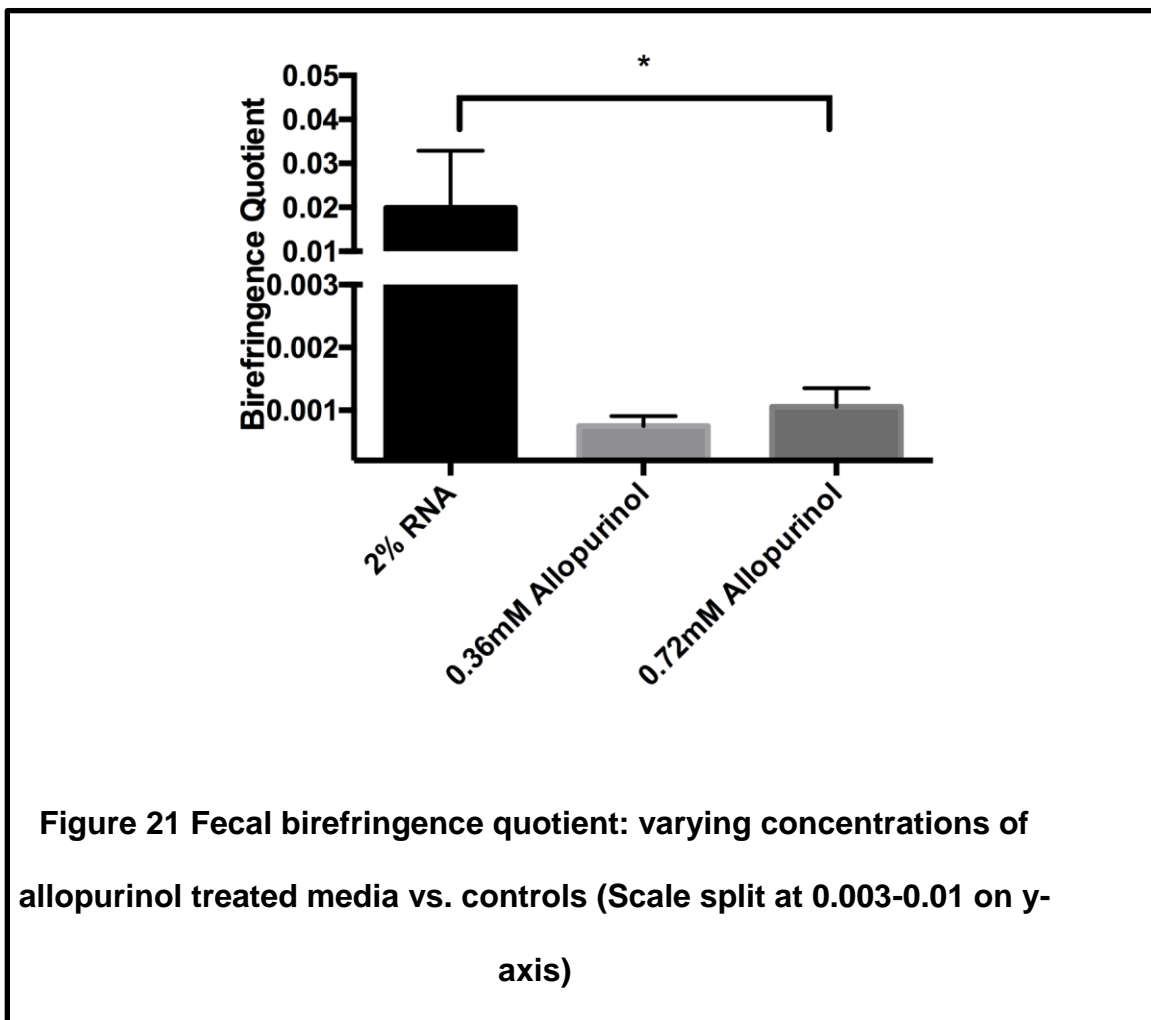
3.4.3 Fecal birefringence under varying purine loads

No significant difference was seen in fecal birefringence between flies fed 1%, 2% and 3% w/v RNA media (One-way ANOVA, Tukey's multiple comparisons $p > 0.05$) (Figure 20).

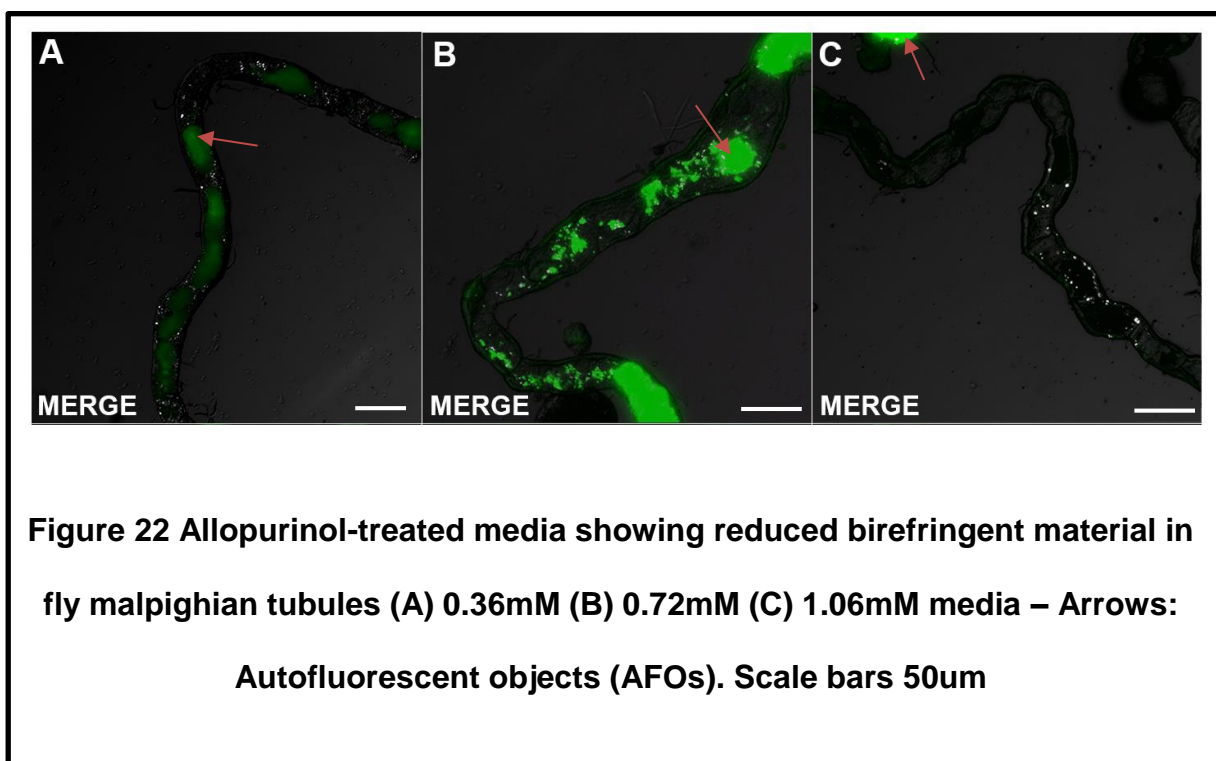


3.4.4 Effect of xanthine oxidase inhibitors on formation of birefringent concretions in fly fecal matter and malpighian tubules

Birefringence quotient was significantly reduced in Allopurinol treated media (0.36mM and 0.72mM Allopurinol) against controls. (One-way ANOVA, Dunnett's multiple comparisons, $p < 0.05$) (**Figure 21**).



To correlate findings with the quantity of birefringent material in fly malpighian tubules, *ex vivo* polarized microscopy was performed after harvesting malpighian tubules from each group. A qualitatively lower quantity of birefringent material was noted at 0.36mM (**Fig 22 – A**), 0.72mM (**Fig 22 – B**) and 1.06mM (**Fig 22 – C**) allopurinol treated media. Surprisingly, autofluorescent objects (AFOs) were observed within the malpighian tubules (arrows) and were more prominently featured in 0.72mM allopurinol media along with structural distortions in the malpighian tubules.



3.4.5 Drug library screening

A pilot high throughput drug screen of 120 plant-derived nutraceutical compounds was conducted and revealed several compounds which appeared to exhibit a reduction in overall fecal birefringence and thus ameliorated crystal formation.

Three compounds appeared to reduce fecal birefringence in a similar manner to allopurinol versus controls. **(Figure 23)**

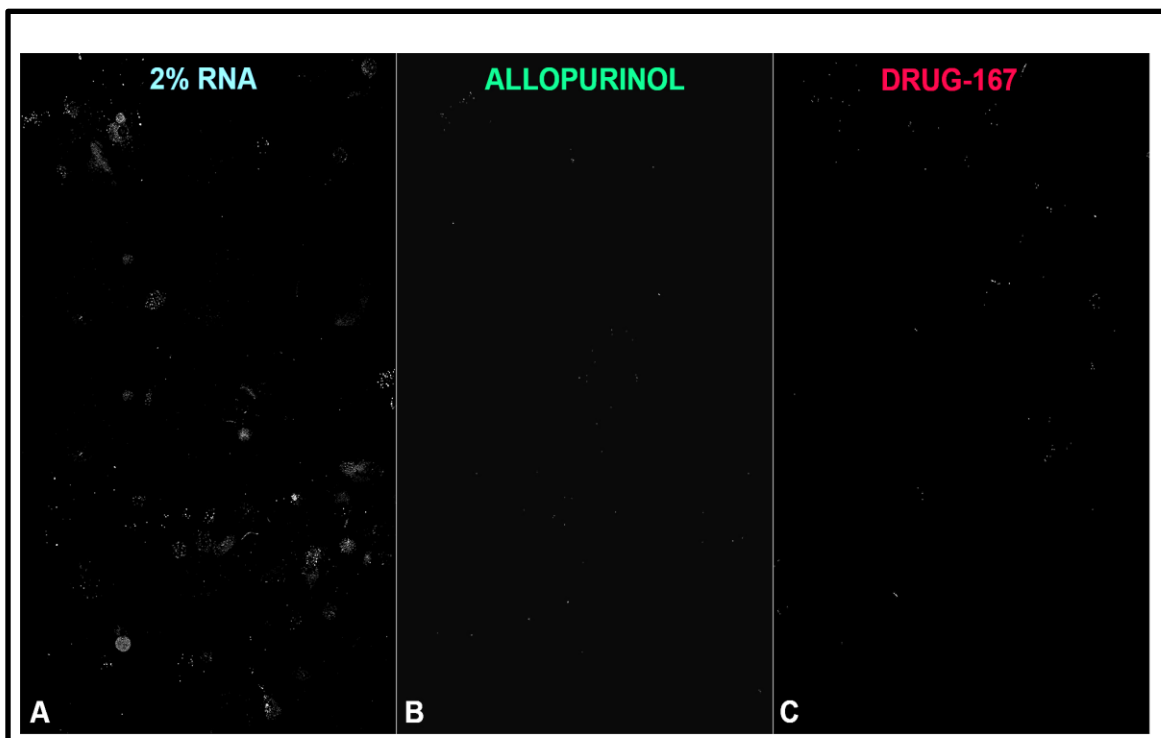


Figure 23 Representative examples: "Yen" algorithm auto-thresholded raw polarized light microscopy images demonstrating fecal birefringence: (A) 2% RNA control (B) Allopurinol (C) test compound "hit". Compressed composite images, whole image brightness increased by 30% to compensate for downscaling.

Chapter 4

4 Discussion and conclusions

This study broadens the role of *Drosophila melanogaster* in the investigation of human nephrolithiasis. Through relatively simple interventions, we demonstrate the formation of uric acid crystals in the malpighian tubules which are readily observed using polarized light microscopy. We also describe a non-invasive semi-quantitative assay involving the imaging of fly fecal matter to determine the effect of bioactive compounds and delineate the role of this model in the high throughput screening of compounds of interest. This was not previously possible due to the constraints of current models of uric acid nephropathy and serves a unique role in narrowing focus for further investigation *in vitro* and in mammalian systems.

4.1 *Ex vivo* imaging of DM malpighian tubules

Confocal microscopy under polarized light showed diffuse brilliantly birefringent crystals in PBac{WH}Uro^{f04888} fly malpighian tubules when fed a high purine diet. As mentioned previously, this fly line contains an amorphic allele for the *Uro* gene (encoding for the enzyme urate oxidase) as a consequence of the mutagenic activity of the transposon *piggyBac*.¹⁵⁴ This fly line has previously been observed to have a strong loss of function *Uro* mutation.¹⁵⁷ The phenomenon of crystal formation can therefore be explained by the disruption of normal purine metabolism. When fed an RNA (or nucleic acid) rich medium, purine nucleotides are liberated by enzymatic degradation in the fly gut; a complex and highly active digestive system.¹⁵⁸ Whilst purines would typically be further metabolized into the more soluble compound allantoin, with significantly reduced urate oxidase activity

this does not occur, resulting in uric acid crystal formation. As *Uro* is almost exclusively expressed in the malpighian tubules^{159,160}, this effect appears to be particularly pronounced in MTs. Importantly, these crystals also appear to either form in or travel between the MTs and the fly gut via the ureteric openings, allowing for detection of birefringent concretions downstream. The initial and transitional segments of the malpighian tubules appear to be more commonly affected, however, this observation may be simply related to the proximity of the main segment to the ureteric orifices and result in crystal migration into the hindgut. In addition, significantly less birefringent material was seen in *Uro*^{f04888} fly MTs fed standard medium. Although no additional yeast-derived RNA was added to this medium, inactivated yeast is a major component of the formulation, which in itself introduces a purine load due to the purine rich nature of yeast.¹⁶¹ No significant differences in crystal formation in fly MTs were qualitatively observed when purine burden was increased suggesting the metabolism of nucleic acids into uric acid may be inhibited beyond a certain threshold. This could potentially occur via end-product non-competitive inhibition. Uric acid, the end-product of purine metabolism in humans, has previously been shown to demonstrate dead-end product inhibition of xanthine oxidase via steady state kinetic analysis.¹⁶² Thus, purine degradation may be reduced or delayed as a result of increased uric acid production and inefficient elimination. Shunting of the intermediate products of purine degradation through an alternative metabolic pathway may also explain these findings however apart from the salvage pathway which recycles the products of purine degradation for *de novo* nucleotide synthesis¹⁶³, such a pathway is yet to be described.

Interestingly, trials involving healthy human participants consuming yeast rich diets have demonstrated a similar effect wherein hyperuricemia and uric acid excretion increase proportionally up to a certain threshold beyond which increasing purine burden does not have a significant effect.¹⁶⁴ It is worth noting that when fed 3% w/v RNA media, fly survival appeared to be significantly impacted. While formal lifespan studies are warranted to confirm this effect, on average at end-point, significantly fewer (n=3) flies survived in the 3% w/v RNA media in comparison to 2% w/v (n=18) and 1% w/v RNA media (n=18). Little to no birefringent concretions were noted in the malpighian tubules of wild-type flies fed standard or purine rich medium reflecting that the disruption of normal purine metabolism appears to be responsible for the formation of birefringent crystal formation in the malpighian tubules. In addition, pilot data was obtained for RNAi-mediated knockdown of the *Uro* gene. Whilst this method of gene silencing did result in birefringent crystal formation, this method required an additional step involving crossing flies prior to investigation, decreasing throughput. Therefore, the *Uro*^{f04888} line was used for future experiments to maximize throughput.

4.2 Quantitative real time PCR and Scanning Electron Microscopy/Energy Dispersive X-ray Spectroscopy

Quantitative real-time PCR showed reduced relative *Uro* gene expression in *Uro*^{f04888} flies relative to wild-type Canton S corresponding to a 74% downregulation in gene expression. This result is consistent with expected results as *Uro*^{f04888} has previously been shown to possess a strong loss of function mutation.¹⁵⁷ *Uro* is almost exclusively expressed in the malpighian tubules and

therefore loss of function corresponds with uric acid crystal accumulation at this site.¹⁵⁹ Broad-spectrum protease mediated dissolution of malpighian tubule tissue in combination with serial washing and centrifugation yielded a clear sample with minimal organic debris appropriate for analysis by SEM. Scanning electron microscopy and energy dispersive X-ray spectroscopy of isolated MT concretions against a pulverized human uric acid calculus both demonstrated similar elemental compositions consisting of carbon (C), nitrogen (N) and oxygen (O), consistent with uric acid. Morphologically, crystalline structures isolated from the malpighian tubules were distinctly smaller in size (~10um) in comparison to the sizes achieved by pulverizing the human uric acid stone sample (~60uM). Additional validation experiments such as biochemical probe assays and high-performance liquid chromatography (HPLC) based detection of uric acid versus controls are warranted to further validate these findings.

4.3 *Ex vivo* imaging of DM fecal matter

Through pilot experiments and our previous work using the calcium oxalate nephrolithiasis model in DM, it was determined that birefringent concretions in fly MTs migrate into the hindgut, the terminal site of fly excretion, via the common ureters. The fly mid and hindgut serve as optimal environments for the continued propagation of uric acid crystallization owing to their acidic pH (<4 and 5, respectively)¹⁵⁸. Thus, we hypothesized fly fecal matter could be utilized to observe variations in stone burden by microscopy under polarized light. Diffuse birefringent concretions were confirmed to be present in Uro^{f04888} fly fecal matter when fed a purine-rich diet. Much smaller areas of birefringence were seen in flies

fed standard medium. No significant differences in fecal birefringence were seen in flies fed 0.1% and 0.2% v/v DMSO medium versus controls. In addition, no significant differences were noted between groups when fed 1%, 2% and 3% w/v RNA media, correlating with observations made during malpighian tubule dissection. To further corroborate these findings, reassessment of these groups with much larger sample sizes would be useful in addition to lifespan studies. To test the effect of a positive control drug on fecal birefringence, the xanthine oxidase inhibitor allopurinol was orally administered to assess if a significant decrease in fecal birefringence could be observed. Oxipurinol, the active form of allopurinol, forms covalent bonds with the active molybdenum site of the enzyme xanthine oxidase forming a oxipurinol-molybdenum complex. This results in the inhibition of enzyme function.^{165,166} Xanthine oxidase is responsible for the conversion of hypoxanthine to xanthine and uric acid. The birefringence per total fecal area was significantly reduced at concentrations of 0.36 and 0.72mM allopurinol in keeping with expected results. Whilst fluorescence confocal microscopy of fly fecal matter allows for higher resolution images with improved contrast along with the capturing of fluorescence data some disadvantages also exist in comparison to traditional light microscopy¹⁶⁷ Images may be limited by the optical penetration of the sample and some scattered light may not be detected. However, traditional microscopy would render determination of total fecal area difficult and the thickness of fecal matter is not likely to be an issue in the majority of cases. Direct comparisons of both imaging techniques over large sample sizes would therefore be useful to assess consistency between methods.

4.4 *Ex vivo* imaging of DM malpighian tubules following Allopurinol treatment

Polarized light confocal microscopy of fly malpighian tubules harvested from Uro^{f04888} flies fed purine rich media containing allopurinol at 0.36mM and 0.72mM concentrations showed significantly reduced birefringent material in MTs. In addition, multiple large autofluorescent objects (AFOs) were noted in the malpighian tubules indiscriminate of tubule segment. In flies fed 0.72mM allopurinol media, large numbers of these bodies were noted along with sections of the MTs where tubule lumen was grossly widened. It has previously been noted that the dietary administration of allopurinol in *Drosophila melanogaster* phenocopies the *ry* (rosy) mutation.¹⁶⁸ The rosy locus encodes for the enzyme xanthine dehydrogenase (XDH) which is responsible for the catalyzing the reaction converting xanthine to uric acid.^{169,170} XDH is interconvertible to xanthine oxidase and both enzymes utilize the same substrates (xanthine, hypoxanthine) but utilize different co-factors.¹⁷⁰ *Ry* mutants have previously been shown to accumulate hypoxanthine and xanthine due to the deficient functioning of XDH.^{171,172} Interestingly, in plant studies investigating point mutations in the xanthine dehydrogenase gene, autofluorescent objects were similarly seen in the mesophyll cells which were found to be rich in xanthine.¹⁷³ It is therefore plausible that the objects visualized in fly malpighian tubules represent xanthine/hypoxanthine particles with the resultant distortions in MT morphology as a result of oxidative stress due to the lack of uric acid production (an anti-oxidant).

4.5 High throughput drug screening

The advantages to the use of *D. melanogaster* as a high throughput drug discovery system have long been known and this process has been described extensively in the literature.^{174–177} Several compounds currently used clinically in a therapeutic role have analogous mechanisms of action in DM and underscores the power of the use of DM in this role.¹⁷⁶ The use of DM however introduces some technical issues as it may only allow for the modelling of a certain facets of human pathology and the interpretation of such assays can be challenging.¹⁷⁸ With these limitations in mind, we have developed a semi-quantitative assay which allows for high throughput screening of bioactive compounds to identify compounds with potential anti-lithogenic effects. These compounds could then be further investigated in mammalian or *in vitro* systems, a process which has not been readily possible through the use of traditional models of uric acid nephropathy.

The method described above involving the *in silico* quantification of birefringence per unit area of fecal matter provides a numerical estimate of relative birefringence. In addition, relative birefringence can be estimated qualitatively, but this process is operator dependent and some training and experience with visualizing raw images is required to make accurate deductions. An aggressive threshold for identifying candidate compounds is therefore warranted as only very large or small relative changes can be determined with accuracy. Through the use of this assay, we have identified three such compounds which appear to reduce fecal birefringence to a level similar to following treatment with the xanthine oxidase inhibitor allopurinol belonging to the bioflavonoid and furanolactone classes of

compounds. At this time, these compounds have not been formally identified for proprietary rights reasons. In addition, due to the nature of the screening process in which each individual drug was screened on a single occasion to assess the utility of this model as a high throughput drug screening system, further investigation of these compounds is warranted to assess if these results can be replicated in this and other mammalian *in vivo* systems.

4.6 Future directions

The genetic tractability, economic efficiency and general ease of use of *D. melanogaster* helps to bridge a fundamental gap in therapeutic drug discovery in nephrolithiasis. The role of DM, however, must be clearly delineated due to the limitations encountered in recapitulating a mammalian system. To strengthen evidence garnered through the use of DM, further investigation in an *in vitro* or mammalian system can be considered. With reference to nephrolithiasis, interest in the direct inhibitors of crystallization is growing. Apart from the recently discovered theobromine and some saponins and glycosaminoglycans, no direct crystallization inhibitors of uric acid nephrolithiasis are known.⁸² During the course of this study, the utility of utilizing *in vitro* grown crystals to perform medium to high throughput drug screens was briefly investigated. We found that large quantities of crystals could be rapidly grown simply *in vitro* through slow evaporation, slow cooling or vapor diffusion. These crystals could also be admixed with fluorescent dyes to allow for direct visualization of crystal morphology (**Figure 24, 25, 26**). In addition, techniques such as turbidimetric assays and visualization under atomic force microscopy (AFM) could be used to investigate morphological changes in

crystal structure under the action of test compounds. These modalities could be utilized as a “pre” or “post” validation screen, further increasing throughput.

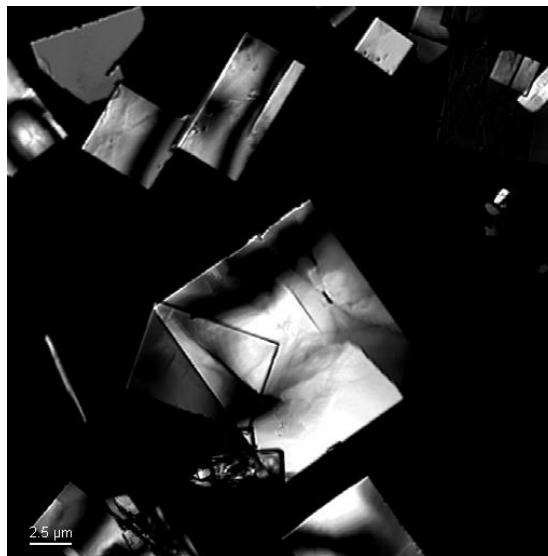


Figure 24 *In vitro* grown uric acid dihydrate (UAD) crystals viewed under polarized light microscopy

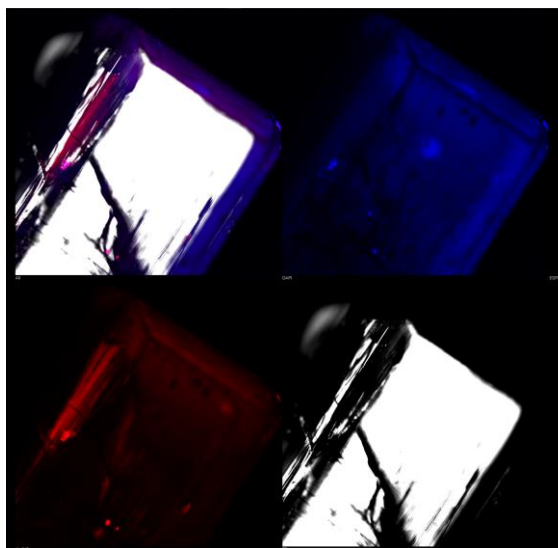


Figure 25 *In vitro* grown L-cystine dihydrochloride crystal admixed with methylene blue under polarized light [DAPI (blue) and Alexa594 (red) channels enabled]

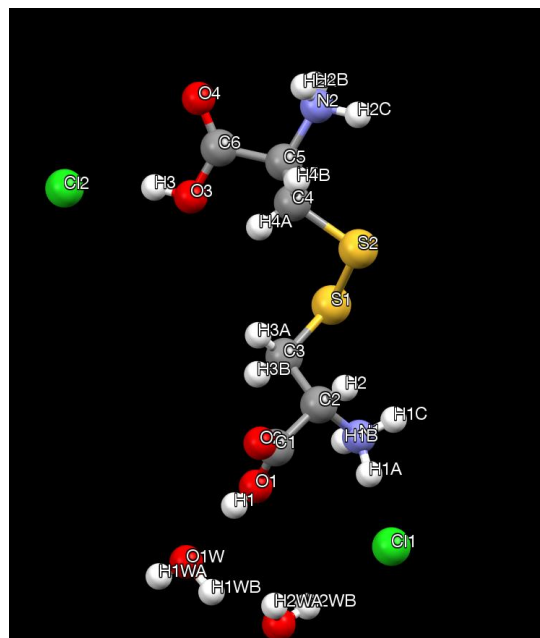


Figure 26 X-ray crystallography of L-cystine based crystal demonstrating characteristic disulfide bond

The use of *in vitro* grown crystals in a similar manner have been previously described in the literature. For example, the role of L-cystine diamides as crystallization inhibitors of cystine crystals was discovered through *in vitro* methods.¹⁷⁹ To improve the robustness of the uric acid model nephrolithiasis and future drug screening, biochemical determination of total uric acid content could be considered through the use of enzymatic assays (Uric Acid Assay Kit, MAK077, Sigma) or high-performance liquid chromatography (HPLC). This would allow for rapid, directly quantifiable result and allow for further validation of the fecal excreta assay described above. In addition, lifespan and survival studies under varying purine loads with and without drug treatments would be beneficial to determine whether any adverse outcomes are observed secondary to crystal formation in MTs. Despite significant efforts, only 45% of the genes significantly enriched in *D.*

melanogaster malpighian tubules have estimates of function.¹⁸⁰ Recent advancements towards expanding our knowledge of the *D. melanogaster* transcriptome in relation to the malpighian tubules have identified several genes which appear to contribute to functionally specific domains such as amino acid transport.¹⁸⁰ Further work in this regard could allow for the development of a *D. melanogaster* model of cystinuria by recapitulating defective cystine transport in the malpighian tubules by the knockdown of these genes; expanding the repertoire of *D. melanogaster* based models of nephrolithiasis. In conclusion, *Drosophila melanogaster* is a promising *in vivo* platform for the modelling of human nephrolithiasis which is not restricted to a single stone subtype. These models also offer an *in vivo* platform for drug screening which is amenable to the application of much larger chemical libraries. The use of birefringent signals to quantitate calculi present in fecal excreta is a key innovation that is cost effective and does not require additional staining or additional processing. This also holds implications in the future, as other birefringent calculi such as cystine calculi would also be amenable to this type of chemical library screen. This screening platform provides several avenues of opportunity to identify additional novel compounds of anti-lithogenic activity, or provide a set of compounds for further evaluation in mammalian pre-clinical models. We are confident the translational potential of these models will hold future promise in the clinic, changing the face of practice in the treatment of nephrolithiasis.

References or Bibliography

1. Pearle, M., Calhoun, E. & Curhan, G. Urologic Diseases In America Project: Urolithiasis. *J. Urol.* **173**, 848–857 (2005).
2. Denstedt, J. D. & Fuller, A. Epidemiology of Stone Disease in North America. in *Urolithiasis* 13–20 (Springer London, 2012). doi:10.1007/978-1-4471-4387-1_2
3. Brikowski, T. H., Lotan, Y. & Pearle, M. S. Climate-related increase in the prevalence of urolithiasis in the United States. *Proc. Natl. Acad. Sci.* **105**, 9841–9846 (2008).
4. Scales, C. D., Smith, A. C., Hanley, J. M. & Saigal, C. S. Prevalence of Kidney Stones in the United States. *Eur. Urol.* **62**, 160–165 (2012).
5. Romero, V., Akpınar, H. & Assimos, D. G. Kidney Stones: A Global Picture of Prevalence, Incidence, and Associated Risk Factors. *Rev. Urol.* **12**, e86–e96 (2010).
6. Saigal, C. S., Joyce, G., Timilsina, A. R. & Urologic Diseases in America Project. Direct and indirect costs of nephrolithiasis in an employed population: opportunity for disease management? *Kidney Int.* **68**, 1808–14 (2005).
7. Foster G, Stocks C, B. M. *Emergency Department Visits and Hospital Admissions for Kidney Stone Disease, 2009: Statistical Brief #139.* (2012).
8. El-Zoghby, Z. M. *et al.* Urolithiasis and the Risk of ESRD. *Clin. J. Am. Soc. Nephrol.* **7**, 1409–1415 (2012).
9. Tang, X. & Lieske, J. C. Acute and chronic kidney injury in nephrolithiasis. *Curr. Opin. Nephrol. Hypertens.* **23**, 385–390 (2014).
10. Alexander, R. T. *et al.* Kidney stones and kidney function loss: a cohort study. *BMJ* **345**, e5287–e5287 (2012).
11. Uribarri, J., Oh, M. S. & Carroll, H. J. The first kidney stone. *Ann. Intern. Med.* **111**, 1006–9 (1989).
12. Moe, O. W. Kidney stones: pathophysiology and medical management. *Lancet* **367**, 333–344 (2006).
13. Worcester, E. M. & Coe, F. L. Calcium Kidney Stones. *N. Engl. J. Med.* **363**, 954–963 (2010).
14. Sakhaee, K., Maalouf, N. M. & Sinnott, B. Kidney Stones 2012: Pathogenesis, Diagnosis, and Management. *J. Clin. Endocrinol. Metab.* **97**, 1847–1860 (2012).
15. Ngo, T. C. & Assimos, D. G. Uric Acid nephrolithiasis: recent progress and future directions. *Rev. Urol.* **9**, 17–27 (2007).
16. Liebman, S. E., Taylor, J. G. & Bushinsky, D. A. Uric acid nephrolithiasis. *Curr. Rheumatol. Rep.* **9**, 251–257 (2007).

17. Iqbal, M. W. *et al.* Should metabolic evaluation be performed in patients with struvite stones? *Urolithiasis* **45**, 185–192 (2017).
18. Mattoo, A. & Goldfarb, D. S. Cystinuria. *Semin. Nephrol.* **28**, 181–191 (2008).
19. Thomas, K., Wong, K., Withington, J., Bultitude, M. & Doherty, A. Cystinuria—a urologist’s perspective. *Nat. Rev. Urol.* **11**, 270–277 (2014).
20. Ramello, A., Vitale, C. & Marangella, M. Epidemiology of nephrolithiasis. *J. Nephrol.* **13 Suppl 3**, S45-50
21. Finkelstein, V. A. Strategies for preventing calcium oxalate stones. *Can. Med. Assoc. J.* **174**, 1407–1409 (2006).
22. Dessombz, A., Letavernier, E., Haymann, J.-P., Bazin, D. & Daudon, M. Calcium Phosphate Stone Morphology Can Reliably Predict Distal Renal Tubular Acidosis. *J. Urol.* **193**, 1564–1569 (2015).
23. Wiederkehr, M. R. & Moe, O. W. Uric Acid Nephrolithiasis: A Systemic Metabolic Disorder. *Clin. Rev. Bone Miner. Metab.* **9**, 207–217 (2011).
24. Akıncı, N., Cakıl, A. & Oner, A. Classical xanthinuria: a rare cause of pediatric urolithiasis. *Türk Üroloji Dergisi/Turkish J. Urol.* **39**, 274–276 (2013).
25. Khan, S. R. Reactive oxygen species, inflammation and calcium oxalate nephrolithiasis. *Transl. Androl. Urol.* **3**, 256–276 (2014).
26. Katsuma, S. *et al.* Global analysis of differentially expressed genes during progression of calcium oxalate nephrolithiasis. *Biochem. Biophys. Res. Commun.* **296**, 544–52 (2002).
27. Sakhaee, K. Recent advances in the pathophysiology of nephrolithiasis. *Kidney Int.* **75**, 585–595 (2009).
28. Rodgers, A. L. Physicochemical mechanisms of stone formation. *Urolithiasis* **45**, 27–32 (2017).
29. Nordin, B. E. & Robertson, W. G. Calcium phosphate and oxalate ion-products in normal and stone-forming urines. *Br. Med. J.* **1**, 450–3 (1966).
30. Finlayson, B. Physicochemical aspects of urolithiasis. *Kidney Int.* **13**, 344–360 (1978).
31. Blomen, L. J. M. J. & Bijvoet, O. L. M. Physicochemical considerations in relation to urinary stone formation. *World J. Urol.* **1**, 119–125 (1983).
32. Aggarwal, K. P., Narula, S., Kakkar, M. & Tandon, C. Nephrolithiasis: Molecular Mechanism of Renal Stone Formation and the Critical Role Played by Modulators. *Biomed Res. Int.* **2013**, 1–21 (2013).
33. Ryall, R. L. The Possible Roles of Inhibitors, Promoters, and Macromolecules in the Formation of Calcium Kidney Stones. in *Urinary Tract Stone Disease* (eds. Rao, N. P., Preminger, G. M. & Kavanagh, J. P.) 31–60 (Springer London, 2011). doi:10.1007/978-1-84800-362-0_4

34. Sugimoto, T. *et al.* Resolution of proteins in the kidney stone matrix using high-performance liquid chromatography. *Eur. Urol.* **11**, 334–40 (1985).
35. Baumann, J. M. From crystalluria to kidney stones, some physicochemical aspects of calcium nephrolithiasis. *World J. Nephrol.* **3**, 256 (2014).
36. Shekarriz, B. & Stoller, M. L. Uric acid nephrolithiasis: current concepts and controversies. *J. Urol.* **168**, 1307–14 (2002).
37. Kumar, A. An Increase Incidence in Uric Acid Nephrolithiasis: Changing Patterns. *J. Clin. DIAGNOSTIC Res.* (2016). doi:10.7860/JCDR/2016/19714.8139
38. Rizvi, S. A. H. *et al.* The management of stone disease. *BJU Int.* **89 Suppl 1**, 62–8 (2002).
39. Hesse, A., Schneider, H. J., Berg, W. & Hienzsch, E. Uric acid dihydrate as urinary calculus component. *Invest. Urol.* **12**, 405–9 (1975).
40. Grenabo, L., Hedelin, H. & Pettersson, S. The severity of infection stones compared to other stones in the upper urinary tract. *Scand. J. Urol. Nephrol.* **19**, 285–9 (1985).
41. Herbstein, F. H., Kleeberg, J., Shalitin, Y., Wartski, E. & Wielinski, S. Chemical and x-ray diffraction analysis of urinary stones in Israel. *Isr. J. Med. Sci.* **10**, 1493–9 (1974).
42. Rafique, M., Bhutta, R. A., Rauf, A. & Chaudhry, I. A. Chemical composition of upper renal tract calculi in Multan. *J. Pak. Med. Assoc.* **50**, 145–8 (2000).
43. Maiuolo, J., Oppedisano, F., Gratteri, S., Muscoli, C. & Mollace, V. Regulation of uric acid metabolism and excretion. *Int. J. Cardiol.* **213**, 8–14 (2016).
44. Usuda, N., Reddy, M. K., Hashimoto, T., Rao, M. S. & Reddy, J. K. Tissue specificity and species differences in the distribution of urate oxidase in peroxisomes. *Lab. Invest.* **58**, 100–11 (1988).
45. Kushiyama, A. *et al.* Role of Uric Acid Metabolism-Related Inflammation in the Pathogenesis of Metabolic Syndrome Components Such as Atherosclerosis and Nonalcoholic Steatohepatitis. *Mediators Inflamm.* **2016**, 1–15 (2016).
46. Wu, X. W., Lee, C. C., Muzny, D. M. & Caskey, C. T. Urate oxidase: primary structure and evolutionary implications. *Proc. Natl. Acad. Sci. U. S. A.* **86**, 9412–6 (1989).
47. Oda, M., Satta, Y., Takenaka, O. & Takahata, N. Loss of urate oxidase activity in hominoids and its evolutionary implications. *Mol. Biol. Evol.* **19**, 640–53 (2002).
48. Johnson, R. J. *et al.* Essential Hypertension, Progressive Renal Disease, and Uric Acid: A Pathogenetic Link? *J. Am. Soc. Nephrol.* **16**, 1909–1919 (2005).

49. Lopez-Torres, M., Perez-Campo, R., Rojas, C., Cadenas, S. & Barja, G. Maximum life span in vertebrates: relationship with liver antioxidant enzymes, glutathione system, ascorbate, urate, sensitivity to peroxidation, true malondialdehyde, in vivo H₂O₂, and basal and maximum aerobic capacity. *Mech. Ageing Dev.* **70**, 177–99 (1993).
50. Inouye, E., Park, K. S. & Asaka, A. Blood uric acid level and IQ: a study in twin families. *Acta Genet. Med. Gemellol. (Roma)*. **33**, 237–42 (1984).
51. Moe, O. W. Uric acid nephrolithiasis: proton titration of an essential molecule? *Curr. Opin. Nephrol. Hypertens.* **15**, 366–373 (2006).
52. Enomoto, A. *et al.* Molecular identification of a renal urate–anion exchanger that regulates blood urate levels. *Nature* **417**, 447–52 (2002).
53. Levinson, D. J. & Sorensen, L. B. Renal handling of uric acid in normal and gouty subject: evidence for a 4-component system. *Ann. Rheum. Dis.* **39**, 173–9 (1980).
54. Maesaka, J. K. & Fishbane, S. Regulation of renal urate excretion: a critical review. *Am. J. Kidney Dis.* **32**, 917–33 (1998).
55. Lipkowitz, M. S. Regulation of Uric Acid Excretion by the Kidney. *Curr. Rheumatol. Rep.* **14**, 179–188 (2012).
56. Ngo, T. C. & Assimos, D. G. Uric Acid nephrolithiasis: recent progress and future directions. *Rev. Urol.* **9**, 17–27 (2007).
57. Pak, C. Y. C., Sakhaee, K., Peterson, R. D., Poindexter, J. R. & Frawley, W. H. Biochemical profile of idiopathic uric acid nephrolithiasis. *Kidney Int.* **60**, 757–761 (2001).
58. Khatchadourian, J., Preminger, G. M., Whitson, P. A., Adams-Huet, B. & Pak, C. Y. Clinical and biochemical presentation of gouty diathesis: comparison of uric acid versus pure calcium stone formation. *J. Urol.* **154**, 1665–9 (1995).
59. Maalouf, N. M., Cameron, M. A., Moe, O. W. & Sakhaee, K. Novel insights into the pathogenesis of uric acid nephrolithiasis. *Curr. Opin. Nephrol. Hypertens.* **13**, 181–9 (2004).
60. Finlayson, B. & Smith, A. Stability of first dissociable proton of uric acid. *J. Chem. Eng. Data* **19**, 94–97 (1974).
61. Menon M, R. M. Urinary lithiasis: etiology, diagnosis, and medical management. *Walsh PC, Ed. Campbell's Urol. 8th ed* 3229–3305 (2002).
62. Flier, J. S., Moore, M. J., Wilson, J. M., Young, A. B. & Kelley, W. N. Hypoxanthine-Guanine Phosphoribosyltransferase Deficiency. *N. Engl. J. Med.* **309**, 900–910 (1983).
63. Borghi, L. *et al.* Hot occupation and nephrolithiasis. *J. Urol.* **150**, 1757–60 (1993).
64. Tsimberidou, A.-M. & Keating, M. J. Hyperuricemic syndromes in cancer

- patients. *Contrib. Nephrol.* **147**, 47–60 (2005).
65. Abate, N. The metabolic syndrome and uric acid nephrolithiasis: Novel features of renal manifestation of insulin resistance. *Kidney Int.* **65**,
 66. Sakhaee, K. Metabolic Syndrome and Uric Acid Nephrolithiasis. *Semin. Nephrol.* **28**, (2008).
 67. Checherita, I. A. FP108RELATIONSHIP BETWEEN URIC ACID NEPHROLITHIASIS AND OBESITY. *Nephrol. Dial. Transplantation* **30**, (2015).
 68. Eskelinen, M., Ikonen, J. & Lipponen, P. Usefulness of history-taking, physical examination and diagnostic scoring in acute renal colic. *Eur. Urol.* **34**, 467–73 (1998).
 69. Halabe, A. & Sperling, O. Uric acid nephrolithiasis. *Miner. Electrolyte Metab.* **20**, 424–31 (1994).
 70. Ombra, M. N. *et al.* Identification of a new candidate locus for uric acid nephrolithiasis. *Am. J. Hum. Genet.* **68**, 1119–29 (2001).
 71. Dalrymple, N. C. *et al.* The value of unenhanced helical computerized tomography in the management of acute flank pain. *J. Urol.* **159**, 735–40 (1998).
 72. Usman, K. D. MP20-11 URINARY STONE CHEMICAL ANALYSIS VS. INFRARED SPECTROSCOPY: A MICRO-CT ASSISTED COMPARATIVE BI-CENTER STUDY. **191**,
 73. Kenny, J.-E. S. & Goldfarb, D. S. Update on the pathophysiology and management of uric acid renal stones. *Curr. Rheumatol. Rep.* **12**, 125–9 (2010).
 74. Moran, M. E., Abrahams, H. M., Burday, D. E. & Greene, T. D. Utility of oral dissolution therapy in the management of referred patients with secondarily treated uric acid stones. *Urology* **59**, 206–10 (2002).
 75. Kursh, E. D. & Resnick, M. I. Dissolution of uric acid calculi with systemic alkalization. *J. Urol.* **132**, 286–7 (1984).
 76. Preminger, G. M. Pharmacologic treatment of uric acid calculi. *Urol. Clin. North Am.* **14**, 335–8 (1987).
 77. Bernardo, N. O. & Smith, A. D. Chemolysis of urinary calculi. *Urol. Clin. North Am.* **27**, 355–65 (2000).
 78. Moran, M. E. Uric acid stone disease. *Front. Biosci.* **8**, s1339-55 (2003).
 79. Borghi, L. *et al.* Urinary volume, water and recurrences in idiopathic calcium nephrolithiasis: a 5-year randomized prospective study. *J. Urol.* **155**, 839–43 (1996).
 80. Xu, H., Zisman, A. L., Coe, F. L. & Worcester, E. M. Kidney stones: an update on current pharmacological management and future directions. *Expert Opin. Pharmacother.* **14**, 435–447 (2013).

81. Seltzer, M. A., Low, R. K., McDonald, M., Shami, G. S. & Stoller, M. L. Dietary manipulation with lemonade to treat hypocitraturic calcium nephrolithiasis. *J. Urol.* **156**, 907–9 (1996).
82. Grases, F., Rodriguez, A. & Costa-Bauza, A. Theobromine Inhibits Uric Acid Crystallization. A Potential Application in the Treatment of Uric Acid Nephrolithiasis. *PLoS One* **9**, e111184 (2014).
83. Gary Curhan, M. A. B. Uric acid nephrolithiasis - UpToDate. *UpToDate* Topic 7378, Version 14 (2017). Available at: <https://www.uptodate.com/contents/uric-acid-nephrolithiasis>. (Accessed: 15th June 2017)
84. Beara-Lasic, L., Pillinger, M. H. & Goldfarb, D. S. Advances in the management of gout: critical appraisal of febuxostat in the control of hyperuricemia. *Int. J. Nephrol. Renovasc. Dis.* **3**, 1–10 (2010).
85. Chen, C., Lü, J.-M. & Yao, Q. Hyperuricemia-Related Diseases and Xanthine Oxidoreductase (XOR) Inhibitors: An Overview. *Med. Sci. Monit.* **22**, 2501–12 (2016).
86. ABELES, A. M. Febuxostat Hypersensitivity. *J. Rheumatol.* **39**, 659–659 (2012).
87. CHOHAN, S. Safety and Efficacy of Febuxostat Treatment in Subjects with Gout and Severe Allopurinol Adverse Reactions. *J. Rheumatol.* **38**, 1957–1959 (2011).
88. Carvalho, M., Lulich, J. P., Osborne, C. A. & Nakagawa, Y. Role of urinary inhibitors of crystallization in uric acid nephrolithiasis: Dalmatian dog model. *Urology* **62**, 566–570 (2003).
89. Schaible, R. H. Genetic predisposition to purine uroliths in Dalmatian dogs. *Vet. Clin. North Am. Small Anim. Pract.* **16**, 127–31 (1986).
90. Bannasch, D. L., Ling, G. V., Bea, J. & Famula, T. R. Inheritance of Urinary Calculi in the Dalmatian. *J. Vet. Intern. Med.* **18**, 483–487 (2004).
91. Bannasch, D. *et al.* Mutations in the SLC2A9 Gene Cause Hyperuricosuria and Hyperuricemia in the Dog. *PLoS Genet.* **4**, e1000246 (2008).
92. Simkin, P. A. The dalmatian defect: A hepatic endocrinopathy of urate transport. *Arthritis Rheum.* **52**, 2257–2262 (2005).
93. Karmi, N. *et al.* Estimated Frequency of the Canine Hyperuricosuria Mutation in Different Dog Breeds. *J. Vet. Intern. Med.* **24**, 1337–1342 (2010).
94. Syme, H. M. Stones in cats and dogs: What can be learnt from them? *Arab J. Urol.* **10**, 230–9 (2012).
95. Wu, X. *et al.* Hyperuricemia and urate nephropathy in urate oxidase-deficient mice. *Proc. Natl. Acad. Sci. U. S. A.* **91**, 742–6 (1994).
96. Horiuchi, H. *et al.* A comparative study on the hypouricemic activity and potency in renal xanthine calculus formation of two xanthine

- oxidase/xanthine dehydrogenase inhibitors: TEI-6720 and allopurinol in rats. *Res. Commun. Mol. Pathol. Pharmacol.* **104**, 307–19 (1999).
97. Asakawa, S. *et al.* Podocyte Injury and Albuminuria in Experimental Hyperuricemic Model Rats. *Oxid. Med. Cell. Longev.* **2017**, 1–14 (2017).
 98. Stavric, B., Nera, E. A., Johnson, W. J. & Salem, F. A. Uric acid kidney stones induced in rats by oxonic acid, a uricase inhibitor. *Invest. Urol.* **11**, 3–8 (1973).
 99. Khan, S. R. Crystal-induced inflammation of the kidneys: results from human studies, animal models, and tissue-culture studies. *J. Clin. Exp. Nephrol.* **8**, 75–88 (2004).
 100. Waisman, J., Mwasi, L. M., Bluestone, R. & Klinenberg, J. R. Acute hyperuricemic nephropathy in rats. An electron microscopic study. *Am. J. Pathol.* **81**, 367–78 (1975).
 101. Bluestone, R., Waisman, J. & Klinenberg, J. R. Chronic experimental hyperuricemic nephropathy. *Lab. Invest.* **33**, 273–9 (1975).
 102. Mazzali, M. *et al.* Elevated Uric Acid Increases Blood Pressure in the Rat by a Novel Crystal-Independent Mechanism. *Hypertension* **38**, (2001).
 103. Kim, Y. G. *et al.* Involvement of macrophage migration inhibitory factor (MIF) in experimental uric acid nephropathy. *Mol. Med.* **6**, 837–48 (2000).
 104. Hou, S., Zhu, W., Pang, M., Jeffry, J. & Zhou, L. Protective effect of iridoid glycosides from *Paederia scandens* (LOUR.) MERRILL (Rubiaceae) on uric acid nephropathy rats induced by yeast and potassium oxonate. *Food Chem. Toxicol.* **64**, 57–64 (2014).
 105. Nakagawa, T. *et al.* Hyperuricemia Causes Glomerular Hypertrophy in the Rat. *Am. J. Nephrol.* **23**, 2–7 (2002).
 106. Feng, Y. *et al.* Taurine decreased uric acid levels in hyperuricemic rats and alleviated kidney injury. *Biochem. Biophys. Res. Commun.* **489**, 312–318 (2017).
 107. TANG, D.-H. *et al.* Potassium oxonate induces acute hyperuricemia in the tree shrew (<i>Tupaia belangeri chinensis&/i>). *Exp. Anim.* 16–0096 (2017). doi:10.1538/expanim.16-0096
 108. Ashburner, M. & Bergman, C. M. *Drosophila melanogaster*: a case study of a model genomic sequence and its consequences. *Genome Res.* **15**, 1661–7 (2005).
 109. Adams, M. D. *et al.* The genome sequence of *Drosophila melanogaster*. *Science* **287**, 2185–95 (2000).
 110. Bier, E. *Drosophila*, the golden bug, emerges as a tool for human genetics. *Nat. Rev. Genet.* **6**, 9–23 (2005).
 111. Ugur, B., Chen, K. & Bellen, H. J. *Drosophila* tools and assays for the study of human diseases. *Dis. Model. Mech.* **9**, 235–44 (2016).

112. Guan, Z., Buhl, L. K., Quinn, W. G. & Littleton, J. T. Altered gene regulation and synaptic morphology in *Drosophila* learning and memory mutants. *Learn. Mem.* **18**, 191–206 (2011).
113. Kramer, J. M. *et al.* Epigenetic Regulation of Learning and Memory by *Drosophila* EHMT/G9a. *PLoS Biol.* **9**, e1000569 (2011).
114. West, R. J. H., Lu, Y., Marie, B., Gao, F.-B. & Sweeney, S. T. Rab8, POSH, and TAK1 regulate synaptic growth in a *Drosophila* model of frontotemporal dementia. *J. Cell Biol.* **208**, 931–947 (2015).
115. Hong, Y. K. Inhibition of JNK/dFOXO pathway and caspases rescues neurological impairments in *Drosophila* Alzheimer's disease model. **419**,
116. KlimanBoth authors contributed to the work equally., M. Structural mass spectrometry analysis of lipid changes in a *Drosophila* epilepsy model brain. *Mol. Biosyst.* **6**, (2010).
117. Kim, J. Y. Neurodegeneration of *Drosophila* drop-dead mutants is associated with hypoxia in the brain. **11**,
118. Sonoda, J. & Wharton, R. P. *Drosophila* Brain Tumor is a translational repressor. *Genes Dev.* **15**, 762–73 (2001).
119. Bodmer, R. The gene tinman is required for specification of the heart and visceral muscles in *Drosophila*. *Development* **118**, (1993).
120. Schott, J. J. *et al.* Congenital heart disease caused by mutations in the transcription factor NKX2-5. *Science* **281**, 108–11 (1998).
121. Diop, S. B. & Bodmer, R. Gaining Insights into Diabetic Cardiomyopathy from *Drosophila*. *Trends Endocrinol. Metab.* **26**, 618–27 (2015).
122. Das, T. & Cagan, R. *Drosophila* as a Novel Therapeutic Discovery Tool for Thyroid Cancer. *Thyroid* **20**, 689–695 (2010).
123. Phatarphekar, A. & Rokita, S. E. Functional analysis of iodotyrosine deiodinase from *drosophila melanogaster*. *Protein Sci.* **25**, 2187–2195 (2016).
124. He, B. Z. *et al.* Effect of Genetic Variation in a *Drosophila* Model of Diabetes-Associated Misfolded Human Proinsulin. *Genetics* **196**, (2014).
125. Glöckl, I., Blaschke, G. & Vei, M. Validated methods for direct determination of hydroquinone glucuronide and sulfate in human urine after oral intake of bearberry leaf extract by capillary zone electrophoresis. *J. Chromatogr. B. Biomed. Sci. Appl.* **761**, 261–6 (2001).
126. Kohyama-Koganeya, A., Kim, Y.-J., Miura, M. & Hirabayashi, Y. A *Drosophila* orphan G protein-coupled receptor BOSS functions as a glucose-responding receptor: Loss of boss causes abnormal energy metabolism. *Proc. Natl. Acad. Sci.* **105**, 15328–15333 (2008).
127. Lee, K.-A. *Drosophila* as a model for intestinal dysbiosis and chronic inflammatory diseases. **42**,

128. Chen, Y.-H. *et al.* Ethylene glycol induces calcium oxalate crystal deposition in Malpighian tubules: a *Drosophila* model for nephrolithiasis/urolithiasis. *Kidney Int.* **80**, 369–377 (2011).
129. Na, J. Diet-Induced Podocyte Dysfunction in *Drosophila* and Mammals. **12**,
130. Singh, S. R. & Hou, S. X. Multipotent stem cells in the Malpighian tubules of adult *Drosophila melanogaster*. *J. Exp. Biol.* **212**, 413–23 (2009).
131. Miller, J. *et al.* *Drosophila melanogaster* as an Emerging Translational Model of Human Nephrolithiasis. *J. Urol.* **190**, 1648–1656 (2013).
132. Rudrapatna, V. A. *Drosophila* cancer models. **241**,
133. Levine, B. D. *Drosophila* Lung Cancer Models Identify Trametinib plus Statin as Candidate Therapeutic. **14**,
134. Denholm, B. & Skaer, H. Bringing together components of the fly renal system. *Curr. Opin. Genet. Dev.* **19**, 526–32 (2009).
135. Zhang, F. & Chen, X. The *Drosophila* nephrocyte has a glomerular filtration system. *Nat. Rev. Nephrol.* **10**, 491–491 (2014).
136. Weavers, H. *et al.* The insect nephrocyte is a podocyte-like cell with a filtration slit diaphragm. *Nature* **457**, 322–326 (2009).
137. Dow, J. A. T., DAVIES, S. A. & SOÖZEN, M. A. Fluid Secretion by the *Drosophila* Malpighian Tubule. *Am. Zool.* **38**, 450–460 (1998).
138. Ho, C.-Y. Effects of commercial citrate-containing juices on urolithiasis in a *Drosophila* model. **29**,
139. Chi, T. *et al.* A *Drosophila* Model Identifies a Critical Role for Zinc in Mineralization for Kidney Stone Disease. *PLoS One* **10**, e0124150 (2015).
140. Landry, G. M. *et al.* Sulfate and thiosulfate inhibit oxalate transport via a dPrestin (Slc26a6)-dependent mechanism in an insect model of calcium oxalate nephrolithiasis. *Am. J. Physiol. - Ren. Physiol.* **310**, (2016).
141. Fu, Y. *et al.* A *Drosophila* model system to assess the function of human monogenic podocyte mutations that cause nephrotic syndrome. *Hum. Mol. Genet.* **26**, 768–780 (2017).
142. Bellen, H. J., Tong, C. & Tsuda, H. 100 years of *Drosophila* research and its impact on vertebrate neuroscience: a history lesson for the future. *Nat. Rev. Neurosci.* **11**, 514–22 (2010).
143. Venken, K. J. T. & Bellen, H. J. Emerging technologies for gene manipulation in *Drosophila melanogaster*. *Nat. Rev. Genet.* **6**, 167–178 (2005).
144. Venken, K. J. T. & Bellen, H. J. Transgenesis upgrades for *Drosophila melanogaster*. *Development* **134**, (2007).
145. Bosch, J. A., Sumabat, T. M. & Hariharan, I. K. Persistence of RNAi-Mediated Knockdown in *Drosophila* Complicates Mosaic Analysis Yet Enables Highly Sensitive Lineage Tracing. *Genetics* **203**, 109–18 (2016).

146. DasGupta, R. & Gonsalves, F. C. High-Throughput RNAi Screen in *Drosophila*. in 163–184 (2008). doi:10.1007/978-1-60327-469-2_13
147. Duffy, J. B. GAL4 system in *Drosophila*: A fly geneticist's swiss army knife. *genesis* **34**, 1–15 (2002).
148. Lin, S.-C., Chang, Y.-Y. & Chan, C.-C. Strategies for gene disruption in *Drosophila*. *Cell Biosci.* **4**, 63 (2014).
149. Drysdale, R. FlyBase. in 45–59 (2008). doi:10.1007/978-1-59745-583-1_3
150. Assimos, D. Re: Ethylene Glycol Induces Calcium Oxalate Crystal Deposition in Malpighian Tubules: A *Drosophila* Model for Nephrolithiasis/Urolithiasis. *J. Urol.* **187**, 1299–1300 (2012).
151. Dow, J. A. T. & Romero, M. F. *Drosophila* provides rapid modeling of renal development, function, and disease. *Am. J. Physiol. Renal Physiol.* **299**, F1237-44 (2010).
152. Rotstein, B. & Paululat, A. On the Morphology of the *Drosophila* Heart. *J. Cardiovasc. Dev. Dis.* **3**, 15 (2016).
153. Dube, K. A., McDonald, D. G. & O'Donnell, M. J. Calcium homeostasis in larval and adult *Drosophila melanogaster*. *Arch. Insect Biochem. Physiol.* **44**, 27–39 (2000).
154. Flybase. FlyBase Allele Report: Dmel\Uro[f04888]. *FB2017_03* (2017). Available at: <http://flybase.org/reports/FBAl0159557.html>. (Accessed: 29th June 2017)
155. Reilly, R. F., Peixoto, A. J. & Desir, G. V. The Evidence-Based Use of Thiazide Diuretics in Hypertension and Nephrolithiasis. *Clin. J. Am. Soc. Nephrol.* **5**, 1893–1903 (2010).
156. Thibault, S. T. *et al.* A complementary transposon tool kit for *Drosophila melanogaster* using P and piggyBac. *Nat. Genet.* **36**, 283–287 (2004).
157. Logan-Garbisch, T. *et al.* Developmental ethanol exposure leads to dysregulation of lipid metabolism and oxidative stress in *Drosophila*. *G3 (Bethesda)*. **5**, 49–59 (2014).
158. Lemaitre, B. & Miguel-Aliaga, I. The Digestive Tract of *Drosophila melanogaster*. *Annu. Rev. Genet.* **47**, 377–404 (2013).
159. Chintapalli, Venkat; Wang, Jing; Dow, J. FlyAtlas 2013 — Enhanced Interface to the *Drosophila* Expression Atlas. Available at: <http://flyatlas.gla.ac.uk/flyatlas/index.html?maxdisplayed=30&showoptions=showoptions&search=gene&gene=CG7171&radioGene=CGnum>. (Accessed: 4th July 2017)
160. Rajan Katoch^{1, 2*} and Neelam Thakur³. Insect gut nucleases: a challenge for RNA interference mediated insect control strategies. *Int. J. Biochem. Biotechnol.* **1**, pp.198-203 (2012).
161. Kaneko, K., Aoyagi, Y., Fukuuchi, T., Inazawa, K. & Yamaoka, N. Total

- Purine and Purine Base Content of Common Foodstuffs for Facilitating Nutritional Therapy for Gout and Hyperuricemia. *Biol. Pharm. Bull.* **37**, 709–721 (2014).
162. Radi, R., Tan, S., Prodanov, E., Evans, R. A. & Parks, D. A. Inhibition of xanthine oxidase by uric acid and its influence on superoxide radical production. *Biochim. Biophys. Acta* **1122**, 178–82 (1992).
 163. Berg JM, Tymoczko JL, S. L. Purine Bases Can Be Synthesized de Novo or Recycled by Salvage Pathways. in *Biochemistry. 5th edition.* (W H Freeman, 2002).
 164. EDOZIEN, J. C., UDO, U. U., YOUNG, V. R. & SCRIMSHAW, N. S. Effects of High Levels of Yeast Feeding on Uric Acid Metabolism of Young Men. *Nature* **228**, 180–180 (1970).
 165. Okamoto, K., Kusano, T. & Nishino, T. Chemical nature and reaction mechanisms of the molybdenum cofactor of xanthine oxidoreductase. *Curr. Pharm. Des.* **19**, 2606–14 (2013).
 166. Okamoto, K., Eger, B. T., Nishino, T., Pai, E. F. & Nishino, T. Mechanism of Inhibition of Xanthine Oxidoreductase by Allopurinol: Crystal Structure of Reduced Bovine Milk Xanthine Oxidoreductase Bound with Oxipurinol. *Nucleosides, Nucleotides and Nucleic Acids* **27**, 888–893 (2008).
 167. Nwaneshiudu, A. *et al.* Introduction to Confocal Microscopy. *J. Invest. Dermatol.* **132**, 1–5 (2012).
 168. Reaume, A. G., Knecht, D. A. & Chovnick, A. The rosy locus in *Drosophila melanogaster*: xanthine dehydrogenase and eye pigments. *Genetics* **129**, 1099–109 (1991).
 169. Keith, T. P. *et al.* Sequence of the structural gene for xanthine dehydrogenase (rosy locus) in *Drosophila melanogaster*. *Genetics* **116**, 67–73 (1987).
 170. Chung, H. Y. *et al.* Xanthine dehydrogenase/xanthine oxidase and oxidative stress. *Age (Omaha)*. **20**, 127–40 (1997).
 171. Kamleh, M. A., Hobani, Y., Dow, J. A. T. & Watson, D. G. Metabolomic profiling of *Drosophila* using liquid chromatography Fourier transform mass spectrometry. *FEBS Lett.* **582**, 2916–2922 (2008).
 172. MITCHELL, H. K., GLASSMAN, E. & HADORN, E. Hypoxanthine in Rosy and Maroon-like Mutants of *Drosophila melanogaster*. *Science (80-.)*. **129**, (1959).
 173. Hofmann, N. R. Opposing Functions for Plant Xanthine Dehydrogenase in Response to Powdery Mildew Infection: Production and Scavenging of Reactive Oxygen Species. *Plant Cell* **28**, 1001 (2016).
 174. Strange, K. Drug Discovery in Fish, Flies, and Worms. *ILAR J.* **57**, 133–143 (2016).

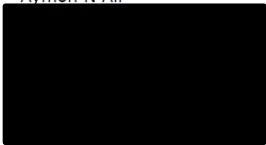
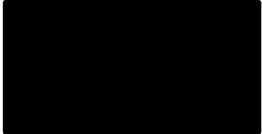
175. Tickoo, S. *Drosophila melanogaster* as a model system for drug discovery and pathway screening. *Curr. Opin. Pharmacol.* **2**, 555–560 (2002).
176. Fernández-Hernández, I., Scheenaard, E., Pollarolo, G. & Gonzalez, C. The translational relevance of *Drosophila* in drug discovery. *EMBO Rep.* **17**, 471–472 (2016).
177. Nichols, C. D. *Drosophila* Models in Therapeutic Drug Discovery Related to Aging. in 213–225 (Springer International Publishing, 2015). doi:10.1007/978-3-319-18326-8_9
178. Pandey, U. B. & Nichols, C. D. Human disease models in *Drosophila melanogaster* and the role of the fly in therapeutic drug discovery. *Pharmacol. Rev.* **63**, 411–36 (2011).
179. Hu, L. *et al.* I -Cystine Diamides as I -Cystine Crystallization Inhibitors for Cystinuria. *J. Med. Chem.* **59**, 7293–7298 (2016).
180. Wang, J. *et al.* Function-informed transcriptome analysis of *Drosophila* renal tubule. *Genome Biol.* **5**, R69 (2004).

Appendices

NATURE PUBLISHING GROUP LICENSE TERMS AND CONDITIONS

Jul 05, 2017

This Agreement between Aymon N Ali ("You") and Nature Publishing Group ("Nature Publishing Group") consists of your license details and the terms and conditions provided by Nature Publishing Group and Copyright Clearance Center.

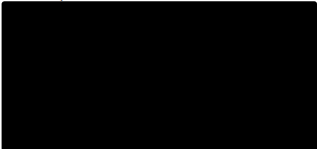
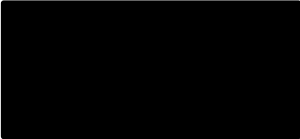
License Number	4137920677122
License date	Jun 28, 2017
Licensed Content Publisher	Nature Publishing Group
Licensed Content Publication	Nature
Licensed Content Title	The insect nephrocyte is a podocyte-like cell with a filtration slit diaphragm
Licensed Content Author	Helen Weavers, Silvia Prieto-Sanchez, Ferdinand Grawe, Amparo Garcia-Lopez, Ruben Artero et al.
Licensed Content Date	Oct 29, 2008
Licensed Content Volume	457
Licensed Content Issue	7227
Type of Use	reuse in a dissertation / thesis
Requestor type	academic/educational
Format	print and electronic
Portion	figures/tables/illustrations
Number of figures/tables/illustrations	1
High-res required	no
Figures	Figure 1, panels (a) to (d)
Author of this NPG article	no
Your reference number	
Title of your thesis / dissertation	The Drosophila melanogaster model of human uric acid nephrolithiasis as a high throughput drug screening tool
Expected completion date	Jul 2017
Estimated size (number of pages)	110
Requestor Location	Aymon N Ali 
Billing Type	Invoice
Billing Address	Aymon N Ali 
Total	0.00 USD

Appendix A 1

**JOHN WILEY AND SONS LICENSE
TERMS AND CONDITIONS**

Jul 05, 2017

This Agreement between Aymon N Ali ("You") and John Wiley and Sons ("John Wiley and Sons") consists of your license details and the terms and conditions provided by John Wiley and Sons and Copyright Clearance Center.

License Number	4137990182631
License date	Jun 28, 2017
Licensed Content Publisher	John Wiley and Sons
Licensed Content Publication	genesis
Licensed Content Title	GAL4 system in drosophila: A fly geneticist's swiss army knife
Licensed Content Author	Joseph B. Duffy
Licensed Content Date	Sep 12, 2002
Licensed Content Pages	15
Type of use	Dissertation/Thesis
Requestor type	University/Academic
Format	Print and electronic
Portion	Figure/table
Number of figures/tables	1
Original Wiley figure/table number(s)	Figure 1
Will you be translating?	No
Title of your thesis / dissertation	The Drosophila melanogaster model of human uric acid nephrolithiasis as a high throughput drug screening tool
Expected completion date	Jul 2017
Expected size (number of pages)	110
Requestor Location	Aymon N Ali 
Publisher Tax ID	EU826007151
Billing Type	Invoice
Billing Address	Aymon N Ali 
Total	0.00 USD

Appendix A 2

**Permission granted via e-mail by Andy Spooner, Communications Assistant,
Company of Biologists (Marked as confidential). Fair use allowed under CC
BY Attribution 4.0 International. "The tiptop/teashirt genes regulate cell differentiation
and renal physiology in *Drosophila*", Denholm et al. Development 2013 140: 1100-1110; doi:
10.1242/dev.088989**

Appendix A 3

Curriculum Vitae

Name: Aymon Ali

Post-secondary Education and Degrees: Khyber Medical University
Peshawar, Pakistan
2007-2013
MBBS (Bachelor of Medicine, Bachelor of Surgery)

The Foundation Programme
Lincoln, United Kingdom
Nottingham, United Kingdom
2013-2016
Postgraduate Clinical Training

Honours and Awards: Western Graduate Research Scholarship (WGRS)
2016-2017

Research Award for Best Poster Presentation (Robert Zhong Research Day)
2017

Related Work Experience MSc in Surgery Candidate
University of Western Ontario
London, ON, Canada
2016-2017

Foundation Clinical Trainee
Lincoln/Nottingham, United Kingdom
2013-2016

Publications:

1. Thamara K Dayarathna, Sohrab N Ali, **Aymon N Ali**, Paul Spagnuolo, Hassan Razvi, Hon S Leong, BRPRS4-7 Arbutin as a novel prevention and therapy for calcium oxalate nephrolithiasis – Accepted at 35th World Congress of Endourology, Vancouver
2. **Aymon N Ali**, Thamara K Dayarathna, Mike Pignanelli, Jihye Kim, Ranjit S Padda, Paul Spagnuolo, Hassan Razvi, Hon S Leong. BRPRS2-6: The Drosophila melanogaster model of human uric acid nephrolithiasis as a

novel in vivo high throughput drug screening platform – Accepted at 35th World Congress of Endourology, Vancouver

3. Sohrab N Ali, Niqad Ahmed, **Aymon N Ali**, Mian Naushad Ali. Emphysematous Pyelonephritis: A review of six cases. J Ayub Med Coll Abbottabad, 2014. Oct-Dec;26(4):591- 7 PMID: 25672195
4. Sohrab N Ali, **Aymon N Ali**, Niqad Ahmed, Mian Naushad Ali. Ureteral triplication and contralateral duplication with vesicoureteral reflux. J Ayub Med Coll Abbottabad. 2014 Apr-Jun;26(2):258- 60 PMID: 25603691
5. Sohrab N Ali, **Aymon N Ali**, Naushad M. Munchausen Syndrome by Proxy – The Overlooked Diagnosis. Ayub Med Coll Abbottabad. 2015 Apr-Jun;27(2):489- 91. PMID: 26411148

Audits and Quality Improvement Projects:

1. 5th National Audit Project (NAP-5) on accidental awareness during general anaesthesia (AAGA), Lincoln County Hospital, County Hospital Louth – Sep 2013, Role: Data collection
2. Clinical Variation in Practice of Laparoscopic Cholecystectomy and Surgical Outcomes: a multi-centre, prospective, population-based cohort study (Choles Study), Role: Data collection

Poster Presentations:

1. **Aymon N Ali**, Thamara Dayarathna, Ranjit Padda, Hassan Razvi, Hon Leong – Novel models of human rare cause nephrolithiasis, Robert Zhong Research Day, London, Ontario
2. **Aymon N Ali**, Thamara Dayarathna, Ranjit Padda, Hassan Razvi, Hong Leong – Novel models of rare cause human nephrolithiasis in *D. melanogaster*, London Health Research Day, London, Ontario

Invited Lectures:

1. JK Wyatt, Urology Residents Research Day
London Convention Centre, London, ON
2. Surgeon's Travel Club
University Hospital, London, ON